Available online at www.sciencedirect.com
SCIENCE DIRECT®
International Journal of Multiphase Flow 31 (2005) 1244–1275
International Journal of Multiphase Flow
www.elsevier.com/locate/ijmulflow

Numerical simulation of a supersonic gas–solid flow over a blunt body: The role of inter-particle collisions and two-way coupling effects

A.N. Volkov [a], Yu.M. Tsirkunov [a], B. Oesterlé [b,*]

[a] *Department of Plasma- and Gasdynamics, Baltic State Technical University, 190005 Saint-Petersburg, Russia*
[b] *LEMTA Laboratory, UMR CNRS 7563, ESSTIN, Henri Poincaré University, 54500 Vandoeuvre-les-Nancy, France*

Received 6 June 2003; received in revised form 12 July 2005

Abstract

A supersonic dusty gas flow over a blunt body is considered. The mathematical model of the two-phase gas–particle flow takes into account the inter-particle collisions and the two-way coupling effects. The carrier gas is treated as a continuum, the averaged flow field of which is described by the complete Navier–Stokes equations with additional source terms modeling the reverse action of the dispersed phase. The dispersed phase is treated as a discrete set of solid particles, and its behavior is described by a kinetic Boltzmann-type equation. Particles impinging on the body surface are assumed to bounce from it. Numerical analysis is carried out for the cross-wise flow over a cylinder. The method of computational simulation represents a combination of a CFD-method for the carrier gas and a Monte Carlo method for the "gas" of particles. The dependence of the fine flow structure of the continuous and dispersed phases upon the free stream particle volume fraction $\alpha_{p\infty}$ and the particle radius r_p is investigated, particularly in the shock layer and in the boundary layer at the body surface. The particle volume fraction $\alpha_{p\infty}$ is varied from a negligibly low value to the value $\alpha_{p\infty} = 3 \times 10^5$ at which inter-particle collisions and two-way coupling effects are simultaneously essential. Particular attention has been given to the particles of radii close to the critical value r_{p*}, because in this range of particle size the behavior of the particles and their effect on the carrier gas flow are not yet completely understood. An estimate of the turbulent kinetic energy produced by the particles in the shock layer is obtained.

* Corresponding author. Tel.: + 33 383 685 080; fax: + 33 383 685 085.
E-mail address: benoit.oesterle@esstin.uhp-nancy.fr (B. Oesterlé).

0301-9322/$ - see front matter © 2005 Elsevier Ltd. All rights reserved.
doi:10.1016/j.ijmultiphaseflow.2005.07.002

Keywords: Dusty gas; Supersonic flow; Blunt body; Boundary layer; CFD/Monte Carlo simulation; Inter-particle collisions; Two-way coupling effects; Turbulence modulation

1. Introduction

The effect of a high-speed two-phase gas–particle flow on a body is of significant interest in many applications such as aircraft and turbine design, industrial processing, etc. As is known, the presence of particles in the free stream, even if their concentration is very low, modifies the flow properties compared with those of a pure gas.

For given body shape and flow parameters, there is a critical value of the particle radius r_{p*} such that particles with smaller radii are decelerated so strongly in the flow field ahead the body that they do not impinge on the body surface (Fuchs, 1964). Particles with radii more than r_{p*} impinge on the body and bounce off the body surface. If the particle concentration in the free stream is not too low, the reflected particles can collide with the incident ones, resulting in the formation of a near-wall layer in which particles move chaotically, colliding with each other. The theoretical a priori estimates show (Tsirkunov, 1993; see also Tsirkunov, 2001) that in the case of coarse-grained particles (the radii of which are much more than r_{p*}) the collisions between incident and reflected particles in the flow over a blunt body can play a noticeable role at very low particle volume fraction in the free stream (at $\alpha_{p\infty} \sim 10^{-6}$). Moreover, the collisions in this case come into play at much lower particle concentration (roughly speaking, 10 times lower) than that at which the reverse effect of the dispersed phase on the carrier gas flow becomes essential. This enables to use the model of one-way coupled flow with particle–particle collisions in a rather wide range of $\alpha_{p\infty}$. On the other hand, this means that a two-way coupled flow model without taking account of inter-particle collisions may be physically incorrect. Nevertheless, it may be mentioned here that two-way coupled flow models with collisionless "gas" of particles (Crowe, 1982; Nigmatulin, 1990) were used to study dusty gas flows with coarse-grained particles over blunt bodies in earlier works (e.g., Golovachov and Schmidt, 1980; Osiptsov, 1985; Ramm, 1988; Ishii et al., 1990).

The importance of collisions between particles in two-phase gas–solid flows has been emphasized by many researchers, mainly in studies of flows in pipes and channels (e.g., Tanaka and Tsuji, 1991; Oesterlé and Petitjean, 1993; Sommerfeld, 1995; Sakiz and Simonin, 2001) and also in analyses of particle dispersion in homogeneous isotropic turbulence (e.g., Zhou et al., 1998; Sommerfeld, 2001). The effect of inter-particle collisions on the wall erosion and heat transfer by particles in an impinging particle-laden jet was studied numerically with the use of the Direct Simulation Monte Carlo (DSMC) method by Kitron et al. (1988).

The paper by Volkov and Tsirkunov (1996) was apparently the first one concerned with the DSMC analysis of inter-particle collisions in the pre-calculated carrier gas flow over a body. Later, Volkov and Tsirkunov (2000) developed the rigorous kinetic model for a "gas" of inelastically and frictionally colliding particles which move in the carrier gas flow. Quite recently, a complete mathematical and computational model for gas–particle flows over bodies with taking account of the inter-particle collisions and the reverse effect of the dispersed phase on the carrier gas was developed (Volkov and Tsirkunov, 2002).

The objective of the present work is to clarify the role of inter-particle collisions and two-way coupling effects in a dusty-gas flow over a blunt body, in particular inside the boundary layer.

The paper describes in detail the models of the gas and dispersed phase flows, including the gas–particle interactions, the particle–particle collisions and the particle–wall impact interactions.

The main assumptions accepted in the present study are the following:

- The particle concentration is low enough for the mutual aerodynamic influence between particles to be negligible.
- The carrier gas is treated as a continuum, the averaged flow field of which is described by the modified complete Navier–Stokes equations.
- The dispersed phase is treated as a discrete set of solid particles which are rigid spheres of equal radii r_p. Particles can interact with each other only through binary collisions. Inter-particle collisions are considered as inelastic and frictional ones.
- The behavior of the set of particles may be described in terms of the one-particle distribution function f_1 which satisfies a kinetic Boltzmann-type equation.
- The action of the carrier gas on every individual particle reduces to some force, torque and heat flux, which can be calculated from the results obtained for an unbounded gas flow around a single particle.
- The reverse action of the particles on the gas can be determined as the sum of the actions of individual particles.

The listed assumptions are not in conflict with each other and they are valid in the flow considered.

For the numerical analysis, a cross-wise supersonic dusty gas flow over a cylinder is taken as an example. The fine flow structure of each phase is studied depending on the free stream particle volume fraction $\alpha_{p\infty}$ and the particle radius r_p. The computational flow model represents a combination of a CFD-method for the carrier gas and a Monte Carlo method for the "gas" of particles. The numerical results illustrate many important features which are common for high-speed two-phase flows over blunt bodies.

2. The model of gas–solid particle flow

2.1. The model of collision between two particles

The main assumption in the formulation of the collision model of a pair of identical dispersed particles is the absence of any persistent particle deformation during a collision. This makes it possible to derive the following relations expressing the particle translational $\mathbf{v}_i$ and rotational $\boldsymbol{\omega}_i$ velocity vectors after the collision in the form proposed by Oesterlé and Petitjean (1993)

$$\mathbf{v}_1^+ = \mathbf{v}_1^- + \frac{\mathbf{J}}{m_p}, \quad \mathbf{v}_2^+ = \mathbf{v}_2^- - \frac{\mathbf{J}}{m_p}, \quad \boldsymbol{\omega}_k^+ = \boldsymbol{\omega}_k^- + \frac{r_p}{I_p}\mathbf{n} \times \mathbf{J}, \quad k = 1, 2, \tag{1}$$

where the superscripts "−" and "+" denote the particle parameters before and after the collision, respectively; r_p is the particle radius, $m_p = (4/3)\pi\rho_p^\circ r_p^3$ and $I_p = (2/5)m_p r_p^2$ are the mass and the

moment of inertia of a particle; ρ_p° is the particle material density; $\mathbf{n}$ is the unit vector directed from the center of the first particle to the center of the second particle; $\mathbf{J}$ is the impulse of forces acting at the contact point of the particle surfaces, determined using an additional hypothesis describing the forces acting at the contact point. Following Babukha and Shraiber (1972), we assume that the relative velocity vectors of the particle surfaces at the contact point, $\mathbf{u} = \mathbf{v}_2 - \mathbf{v}_1 + r_p\mathbf{n}\times(\boldsymbol{\omega}_1 + \boldsymbol{\omega}_2)$, before and after the collision, are connected by $u^+ = -a_{pn}(\mathbf{u}^-\cdot\mathbf{n})\mathbf{n} + a_{pt}(\mathbf{u}^- - (\mathbf{u}^-\cdot\mathbf{n})\mathbf{n})$, where a_{pn} and a_{pt} denote the restitution ratios of the normal and tangential components of $\mathbf{u}$. From physical point of view, these coefficients, whose values belong to the range $0 \leqslant a_{pn}$, $|a_{pt}| \leqslant 1$, account for the inelasticity of collisions and the friction between particle surfaces. The impulse $\mathbf{J}$ can finally be expressed as

$$\mathbf{J} = m_p\left(\frac{1+a_{pn}}{2}(\mathbf{u}^-\cdot\mathbf{n}) + \frac{1-a_{pt}}{7}(\mathbf{u}^- - (\mathbf{u}^-\cdot\mathbf{n})\mathbf{n})\right). \tag{2}$$

According to the results of Sun and Chen (1988) we can neglect the contact heat transfer between particles because the contact area and the impact duration are too small. Nevertheless the particle temperature T_k can change during a collision due to transformation of the part ΔK of kinetic energy into thermal energy U_k of particles, with $\Delta K = K_1^- + K_2^- - (K_1^+ + K_2^+)$, $K_k = m_p\mathbf{v}_k^2/2 + I_p\boldsymbol{\omega}_k^2/2$; $k = 1, 2$. As the particle absolute temperature increases strongly inside the shock layer, the temperature dependence of the particle material specific heat c_p° has to be taken into account. It is written in the form

$$c_p^\circ(T) = a_c\cdot T^3 + b_c\cdot T^2 + C_c\cdot T + d_c, \tag{3}$$

where a_c, b_c, c_c and d_c are empirical constants. Assuming that the additional heat energy distributes equally between the two particles, we have $U_k^+ = U_k^- + \Delta K/2$, $U_k = m_p\int_0^{T_k} c_p^\circ(T)\mathrm{d}T$. Typically the change in particle temperature during a single collision is small enough for the corresponding change in particle specific heat to be neglected, so that

$$T_k^+ = T_k^- + \frac{\Delta K}{2m_p c^\circ(T_k^-)}, \quad k = 1, 2. \tag{4}$$

Denoting $\mathbf{y}_i = (\mathbf{v}_i, \boldsymbol{\omega}_i, T_i)$, the relations (1) and (4) can be formally written in the compact form

$$\mathbf{y}_1^+ = \mathbf{y}_1^+(\mathbf{y}_1^-, \mathbf{y}_2^-, \mathbf{n}), \quad \mathbf{y}_2^+ = \mathbf{y}_2^+(\mathbf{y}_1^-, \mathbf{y}_2^-, \mathbf{n}). \tag{5}$$

2.2. Kinetic description of the collisional dispersed phase

Under the above stated assumptions the state of the ith particle is determined uniquely by the set of its phase coordinates $\mathbf{x}_i = (\mathbf{r}_i, \mathbf{v}_i, \boldsymbol{\omega}_i, T_i) = (\mathbf{r}_i, \mathbf{y}_i)$, where $\mathbf{r}_i$ is the position vector of the particle in the physical space.

Let $\mathbf{r}$ be the position vector of an arbitrary point in the two-phase flow, t the time. By analogy with the kinetic theory of gases we introduce the one-particle distribution function $f_1 = f(\mathbf{x}_1, t) = f(\mathbf{r}_1, \mathbf{y}_1, t)$ normalized by the numerical concentration of particles $n_p(\mathbf{r}, t)$

$$n_p(\mathbf{r}, t) = \int f(\mathbf{r}, \mathbf{y}_1, t)\mathrm{d}\mathbf{y}_1.$$

This function describes the state of the dispersed phase.

Change of the phase coordinates is caused by particle–particle collisions and gas–particle interaction. As stated by Volkov and Tsirkunov (2000), in dense flows with coarse-grained particles the characteristic length and time of particle collisions are several orders smaller than the length and time of particle velocity relaxation in the gas flow field. It is therefore possible to consider the inter-particle collisions as instantaneous ones, and, hence, to take them into account in the dispersed phase kinetic model through the usual collisional integral generalized to the case of inelastically colliding and rotating particles. Under these conditions the action of the carrier gas on a particle can be considered as an external action that determines the particle system evolution. This argument was used by Volkov and Tsirkunov (2000) to derive the basic kinetic equation for the N-particle distribution function. From this basic kinetic equation, in the thermodynamic limit, i.e. N, $V \to \infty$ but $N/V = \text{const}$, where N is the number of particles, V is the volume where they are located, and under the assumption similar to molecular chaos, the Boltzmann-type kinetic equation in terms of f_1 can be derived in the form

$$\frac{\partial f_1}{\partial t} + \frac{\partial}{\partial \mathbf{r}_1} \cdot (\mathbf{v}_1 f_1) + \frac{\partial}{\partial \mathbf{v}_1} \cdot \left(\frac{\mathbf{f}_1}{m_\mathrm{p}} f_1 \right) + \frac{\partial}{\partial \boldsymbol{\omega}_1} \cdot \left(\frac{\mathbf{l}_1}{I_\mathrm{p} f_1} \right) + \frac{\partial}{\partial T_1} \left(\frac{q_1}{m_\mathrm{p}} c_\mathrm{p}^\circ f_1 \right) = I_{12}(f_1), \tag{6}$$

$$I_{12}(f_1) = (2r_\mathrm{p})^2 \int \int_{\mathbf{g}.\mathbf{n} \leqslant 0} \left(\frac{f_1^- f_2^-}{J} - f_1 f_2 \right) |\mathbf{g}.\mathbf{n}| \sin\chi \, \mathrm{d}\chi \, \mathrm{d}\varepsilon \, \mathrm{d}\mathbf{y}_2. \tag{7}$$

Here $\mathbf{f}_1$ and $\mathbf{l}_1$ are the force and the moment exerted on a particle by the carrier gas, q_1 the complete heat flux through the particle surface; $\mathbf{g} = \mathbf{v}_2 - \mathbf{v}_1$ the relative velocity vector between the two particles; χ and ε the spherical angular coordinates defined in such a way that $\mathbf{n} = \cos\chi \mathbf{i} + \sin\chi\cos\varepsilon \mathbf{j} + \sin\chi\sin\varepsilon \mathbf{k}$, where $(\mathbf{i}, \mathbf{j}, \mathbf{k})$ is the basis of the Cartesian coordinate system (x, y, z); $f_2 = f(\mathbf{r}_1, \mathbf{y}_2, t)$, $f_1^- = f(\mathbf{r}_1, \mathbf{y}_1^-(\mathbf{y}_1, \mathbf{y}_2, \mathbf{n}), t)$ and $f_2^- = f(\mathbf{r}_1, \mathbf{y}_2^-(\mathbf{y}_1, \mathbf{y}_2, \mathbf{n}), t)$. The functions $\mathbf{y}_k^-(\mathbf{y}_1, \mathbf{y}_2, \mathbf{n})$ $(k = 1, 2)$, which are inverse to the ones given by (5), determine the values of the phase coordinates of a pair of particles before a collision with given direction of center line $\mathbf{n}$ in order that they acquire the velocities and temperature corresponding to $\mathbf{y}_1$ and $\mathbf{y}_2$.

The parameter J in the collision integral $I_{12}(f_1)$ takes into account the phase volume reduction due to the inelasticity of the collision and is equal to

$$J = \left| \frac{\mathbf{g} \cdot \mathbf{n}}{\mathbf{g}^- \cdot \mathbf{n}} J_1 \right|, \quad J_1 = \left| \frac{\partial(\mathbf{y}_1^+, \mathbf{y}_2^+)}{\partial((\mathbf{y}_1^-, \mathbf{y}_2^-)} \right| \neq 0.$$

Thus the Jacobian J_1 of the transformation (5) is assumed not to be equal to zero. Under this condition the relations (5) can be solved in terms of the particle parameters before collision. For the particle–particle collision model described in the previous section one can derive $J_1 = -a_\mathrm{pn} a_\mathrm{pt}^2$ and $J = a_\mathrm{pn}^2 a_\mathrm{pt}^2$.

The macroparameters of the dispersed phase are the object of main interest in practice. Let $[\Phi](\mathbf{r}, t)$ denote the total value per unit volume of the gas–particle mixture of any quantity $\Phi = \Phi(\mathbf{x}_1)$ of an individual particle. By analogy with the kinetic theory of gases the macroparameter $[\Phi](\mathbf{r}, t)$ can be expressed as a statistically averaged value

$$[\Phi](\mathbf{r}, t) = \int \Phi(\mathbf{r}, \mathbf{y}_1) f(\mathbf{r}, \mathbf{y}_1, t) \mathrm{d}\mathbf{y}_1. \tag{8}$$

Then the numerical and volumetric concentrations of the dispersed phase are defined as $n_p = [1]$, $\alpha_p = (4/3)\pi r_p^3 n_p$. The ratio of the average value of the molecular parameter in the unit volume of the gas–particle mixture, $[\Phi]$, to the average number of particles in the unit volume, n_p, gives the average value of the molecular parameter $[\Phi]_l = [\Phi]/n_p$ for a single particle. For instance, the macroscopic velocity of the particle phase $\mathbf{u}_p$ is determined by $\mathbf{u}_p = [\mathbf{v}_1]_l$.

The flux per unit surface area $[\Phi]_w$ of the physical parameter Φ from the dispersed phase towards the stationary body surface at a point $\mathbf{r}_w$ is defined as follows:

$$[\Phi]_w(\mathbf{r}_w, t) = -\int (\mathbf{v}_1.\mathbf{n}_w)\Phi(\mathbf{r}_w, \mathbf{y}_1) f(\mathbf{r}_w, \mathbf{y}_1, t)\mathrm{d}\mathbf{y}_1. \tag{9}$$

Here $\mathbf{n}_w$ is the unit vector normal to the surface, directed from the body to the fluid. By analogy with (8) the value of the flux density can be formally represented in the form $[\Phi]_w = [-(\mathbf{v}_1 \cdot \mathbf{n}_w)\Phi]$. For example, the quantity e_w giving the upper-bound estimate of the energy flux density from the dispersed particles to the body surface due to the inelasticity of particle rebound from the surface, is defined as $e_w = [K_1 + U_1]_w$.

2.3. Gas–particle interaction

Many different models describing the interaction of a carrier gas with individual particles are known in the literature (see e.g., Nigmatulin, 1990; Crowe et al., 1998). In most cases however, they are applied to incompressible subsonic flows in pipes or channels. In case of supersonic flow of viscous gas–particle mixture over bodies it is necessary to take into account the compressibility of the carrier gas in the flow over a single particle and the rarefaction of the gas flow associated with the fact that the mean free path of gas molecules can be of the same order as the particle radius r_p.

In general, we should also consider the near-wall effects associated with the non-isothermal shear flow inside the boundary layer and the constrained flow over a particle near the surface. The boundary layer effects are usually taken into account by means of additional terms in the interphase interaction force, namely, the Saffman force, the thermophoretic force and the "wall effect" (see the paper by Tsirkunov et al., 1994a). A preliminary study was carried out to estimate the role of these various contributions in the interphase interaction term $\mathbf{f}_1$; showing that the effects of such near-wall forces on the dispersed phase motion are not significant in the range of parameters considered below. Based on this fact, only the drag force $\mathbf{f}_D$ and the Magnus lift force $\mathbf{f}_M$ that arises from the collision induced spinning motion of the particle are taken into account in the following, so that

$$\mathbf{f}_1 = \mathbf{f}_D + \mathbf{f}_M, \tag{10}$$

where

$$\mathbf{f}_D = \frac{1}{2} C_D \pi r_p^2 \rho |\mathbf{v} - \mathbf{v}_1|(\mathbf{v} - \mathbf{v}_1), \quad \mathbf{f}_M = C_\omega \pi r_p^3 \rho (\boldsymbol{\omega} - \boldsymbol{\omega}_1) \times (\mathbf{v} - \mathbf{v}_1). \tag{11}$$

The damping torque $\mathbf{l}_1$ and the heat flux q_1 through the particle surface are expressed as usually:

$$\mathbf{l}_1 = \frac{1}{2} C_l r_p^5 \rho |\boldsymbol{\omega} - \boldsymbol{\omega}_1|(\boldsymbol{\omega} - \boldsymbol{\omega}_1), \quad q_1 = 2Nu_p \pi r_p \kappa^*(T - T_1). \tag{12}$$

Here $\mathbf{v}$, ρ, T and κ^* are the velocity vector, the temperature, the density and the heat conduction of the carrier gas, and $\boldsymbol{\omega} = (1/2)\nabla \times \mathbf{v}$.

The coefficients C_D, C_ω, C_l and Nu_p in (11) and (12) are defined from semi-empirical correlations in terms of the Mach number $M_1 = |\mathbf{v} - \mathbf{v}_1|/\sqrt{\gamma \Re T}$ and the Reynolds numbers based on relative translational velocity $Re_1 = 2r_p\rho|\mathbf{v} - \mathbf{v}_1|/\mu$ and relative rotational velocity $Re_{\omega 1} = 4r_p^2\rho|\boldsymbol{\omega} - \boldsymbol{\omega}_1|/\mu$ (here $\Re = c_p - c_v$ is the gas constant, $\gamma = c_p/c_v$, c_v and c_p are the gas specific heats under constant volume and constant pressure, respectively, μ, is the gas viscosity). The drag coefficient C_D is determined by the Henderson (1976) relations $C_D = C_D(Re_1, M_1, T_1/T, \gamma)$, which takes into account the inertial effects, the compressibility and the rarefaction of the gas in the flow over a sphere and is valid in a wide range of Mach number and Reynolds number (i.e. $M_1 \leqslant 6$ and $Re_1 \leqslant 10^5$). The coefficient in the Magnus lift force C_ω is expressed by $C_\omega = C_\omega(Re_1, Re_{\omega 1})$ for $\delta = Re_{\omega 1}/Re_1 \geqslant 0.45$, according to the relation given by Oesterlé and Bui Dinh (1998), and $C_\omega = 1$ for $\delta \leqslant 0.45$, which is the theoretical solution of Rubinow and Keller (1961). The torque coefficient $C_l = C_l(Re_{\omega 1})$ is calculated by the correlations of Dennis et al. (1980), and the Nusselt number $Nu_p = Nu_p(Re_1, M_1, Pr)$ by the Kavanau formula

$$Nu_p = \frac{Nu_p^0}{1 + 3.42 Nu_p^0 M_1/(Re_1 Pr)}, \tag{13}$$

where $Nu_p^0 = 2 + 0.459 Re_1^{0.55} Pr^{0.33}$ is the Nusselt number for the continuum flow regime; the coefficient of order of the Knudsen number M_1/Re_1 takes into account the influence of the gas rarefaction on the heat transfer (see Sternin and Shraiber, 1994), and $Pr = c_p\mu/\kappa^*$ is the Prandtl number.

2.4. Governing equations for the carrier gas flow

The Navier–Stokes equations for ideal viscous compressible gas are used to describe the carrier gas "micro" flow in the gaps between particles. They include the continuity, momentum and energy equations:

$$\frac{\partial \rho}{\partial t} + \nabla \cdot (\rho \mathbf{v}) = 0, \tag{14}$$

$$\frac{\partial}{\partial t}(\rho \mathbf{v}) + \nabla \cdot (\rho \mathbf{v}\mathbf{v}) = \nabla \cdot \boldsymbol{\Sigma}, \tag{15}$$

$$\frac{\partial}{\partial t}(\rho e) + \nabla \cdot (\rho \mathbf{v} e) = -\nabla \cdot \mathbf{q} + \nabla \cdot (\boldsymbol{\Sigma} \cdot \mathbf{v}). \tag{16}$$

Here $\boldsymbol{\Sigma}$ and $\mathbf{q}$ are the stress tensor and the heat flux vector determined by Newton's and Fourier's laws

$$\boldsymbol{\Sigma} = (-p - (2/3)\mu \nabla \cdot \mathbf{v})\mathbf{I} + 2\mu \mathbf{S}, \quad \mathbf{q} = -\kappa^* \nabla T, \tag{17}$$

where $\mathbf{S}$ is the gas deformation tensor, $\mathbf{I}$ the unit (metric) tensor, p the pressure and e the total energy of the gas, the viscosity μ and the heat conduction κ^* being defined by the Sutherland formula, i.e.

$$p = \rho \Re T, \quad e = c_v T + \frac{\mathbf{v}^2}{2}, \quad \mu = \mu_s \left(\frac{T}{T_s}\right)^{3/2} \frac{T_s + C_s}{T + C_s}, \quad \kappa^* = \frac{c_p \mu}{Pr}. \tag{18}$$

As usually, we use the hypothesis that in every point $\mathbf{r}$ of the flow one can define a physically infinitesimal control volume $D(\mathbf{r})$ whose length scale is much more than the mean distance between particles l_p but much less than the length scale of the flow R. Then to derive the averaged equations of the carrier gas we can use the volume average procedure described in details by Nigmatulin (1990) and Crowe et al. (1998). The volume averaged value $\bar{f}$ of any flow parameter f is defined as

$$\bar{f}(\mathbf{r},t)=\frac{1}{V}\int_{D_c(\mathbf{r},t)} f(\tilde{\mathbf{r}},t)\mathrm{d}\tilde{\mathbf{r}},\quad \alpha_c=\frac{V_c}{V},\quad V_c=\int_{D_c(\mathbf{r},t)}\mathrm{d}\tilde{\mathbf{r}}, \tag{19}$$

where V is the volume of D, D_c the part of control volume free of particles, α_c the gas volume fraction. In addition we introduce the phase averaged $\{f\}$ and mass averaged $\langle f\rangle$ values of the parameter f:

$$\{f\}(\mathbf{r},t)=\frac{1}{V_c}\int_{D_c(\mathbf{r},t)} f(\tilde{\mathbf{r}},t)\mathrm{d}\tilde{\mathbf{r}}=\frac{\bar{f}}{\alpha_c},\quad \langle\rho\rangle=\alpha_c\{\rho\},\quad \langle f\rangle=\frac{\{\rho f\}}{\langle\rho\rangle} \tag{20}$$

and represent the velocity $\mathbf{v}$ and the temperature T of the carrier gas as the sums of mass-averaged values $\langle\mathbf{v}\rangle$ and $\langle T\rangle$ and fluctuations $\mathbf{v}'$ and T': $\mathbf{v}=\langle\mathbf{v}\rangle+\mathbf{v}'$, $T=\langle T\rangle+T'$.

In order to express the averaged values of the derivatives (e.g., $\overline{\partial f/\partial x}$) by means of the derivatives of the averaged values (e.g., $\partial\{f\}/\partial x$) one can use the integral theorem which leads to

$$\overline{\frac{\partial f}{\partial t}}=\frac{\partial}{\partial t}(\alpha_c\{f\})+\frac{1}{V}\int_{S_p} f\mathbf{v}\cdot\mathbf{n}_i\,\mathrm{d}S,\quad \overline{\frac{\partial f}{\partial \beta}}=\frac{\partial}{\partial \beta}(\alpha_c\{f\})-\frac{1}{V}\int_{S_p} f n_{i\beta}\mathrm{d}S\quad(\beta=x,y,z),$$

where $S_p=\cup S_i$, S_i is the part of the surface of the ith particle immersed within the control volume D, $n_{i\beta}$ the components of unit vector $\mathbf{n}_i$, which is normal to the surface of the ith particle and directed from the particle to the fluid.

Applying the volume average procedure (19) to all terms in Eqs. (14)–(16) we get the following averaged equations:

$$\frac{\partial\langle\rho\rangle}{\partial t}+\nabla\cdot(\langle\rho\rangle\langle\mathbf{v}\rangle)=0, \tag{21}$$

$$\frac{\partial}{\partial t}(\langle\rho\rangle\langle\mathbf{v}\rangle)+\nabla\cdot(\langle\rho\rangle\langle\mathbf{v}\rangle\langle\mathbf{v}\rangle)=\nabla\cdot(\alpha_c\{\boldsymbol{\Sigma}\})-\nabla\cdot(\langle\rho\rangle\langle\mathbf{v}'\mathbf{v}'\rangle)+\boldsymbol{\Pi}_m, \tag{22}$$

$$\begin{aligned}\frac{\partial}{\partial t}(\langle\rho\rangle\langle e\rangle)+\nabla\cdot(\langle\rho\rangle\langle\mathbf{v}\rangle\langle e\rangle)=&-\nabla.(\alpha_c\{\mathbf{q}\})+\nabla\cdot(\alpha_c\{\boldsymbol{\Sigma}\}\cdot\langle\mathbf{v}\rangle)+\nabla\cdot(\alpha_c\{\boldsymbol{\Sigma}\cdot\mathbf{v}'\})\\&+\Pi_{e\Sigma}+\Pi_{eq}-\nabla\cdot(\langle\rho\rangle\langle\mathbf{v}\rangle\cdot\langle\mathbf{v}'\mathbf{v}'\rangle)-\nabla\cdot\left(\langle\rho\rangle\left\langle\mathbf{v}'\frac{(\mathbf{v}')^2}{2}\right\rangle\right)\\&\times\nabla\cdot(\langle\rho\rangle c_v\langle\mathbf{v}'T'\rangle).\end{aligned} \tag{23}$$

Here the source term $\boldsymbol{\Pi}_m$ is the averaged force exerted on the gas by the particles, per unit volume:

$$\boldsymbol{\Pi}_m=-\frac{1}{V}\int_{S_p}\boldsymbol{\Sigma}\cdot\mathbf{n}_i\,\mathrm{d}S=-\frac{1}{V}\sum_i\int_{S_i}\boldsymbol{\Sigma}\cdot\mathbf{n}_i\,\mathrm{d}S=-\frac{1}{V}\sum_i\mathbf{f}_i, \tag{24}$$

$\Pi_{e\Sigma}$ is the power produced by stresses on the particle surfaces, and Π_{eq} is the heat flux at the particle surfaces, both per unit volume:

$$\Pi_{e\Sigma} = -\frac{1}{V}\int_{S_\mathrm{p}} \mathbf{W}_i \cdot \boldsymbol{\Sigma} \cdot \mathbf{n}_i \,\mathrm{d}S = -\frac{1}{V}\sum_i (\mathbf{f}_i \cdot \mathbf{v}_i + \mathbf{l}_i \cdot \boldsymbol{\omega}_i),$$
$$\Pi_{\mathrm{eq}} = -\frac{1}{V}\int_{S_\mathrm{p}} \mathbf{q} \cdot \mathbf{n}_i \,\mathrm{d}S = -\frac{1}{V}\sum_i q_i, \tag{25}$$

where $\mathbf{W}_i = \mathbf{v}_i + r_\mathrm{p}\boldsymbol{\omega}_i \times \mathbf{n}_i$ is the velocity at the surface of the ith particle. The average total energy $\langle e\rangle$ in (23) includes the average kinetic energy of the gas velocity fluctuations k:

$$\langle e\rangle = \frac{\langle \mathbf{v}\rangle^2}{2} + k + c_\mathrm{v}\langle T\rangle, \quad k = \frac{\langle(\mathbf{v}')^2\rangle}{2}. \tag{26}$$

We derive the turbulent kinetic energy equation in the same manner as Kenning and Crowe (1997). Multiplying Eq. (22) by $\langle \mathbf{v}\rangle$, the mean kinetic energy equation is obtained, then the momentum equation (15) multiplied by $\mathbf{v}$ is averaged and the mean kinetic energy equation is subtracted from it, resulting in

$$\frac{\partial}{\partial t}(\langle\rho\rangle k) + \nabla\cdot(\langle\rho\rangle\langle\mathbf{v}\rangle k) = -\langle\rho\rangle\langle\mathbf{v}'\mathbf{v}'\rangle : \nabla\langle\mathbf{v}\rangle + \nabla\cdot(\alpha_\mathrm{c}\{\boldsymbol{\Sigma}.\mathbf{v}'\})$$
$$+ \alpha_\mathrm{c}\{\boldsymbol{\Sigma}\} : \nabla\langle\mathbf{v}\rangle - \nabla\cdot\left(\langle\rho\rangle\left\langle \mathbf{v}'\frac{(\mathbf{v}')^2}{2}\right\rangle\right) - \alpha_\mathrm{c}\{\boldsymbol{\Sigma} : \nabla\mathbf{v}\} + \Pi_k, \tag{27}$$

where it is assumed that the term Π_k, defined by

$$\Pi_k = \Pi_{e\Sigma} - \boldsymbol{\Pi}_m \cdot \langle\mathbf{v}\rangle = -\frac{1}{V}\sum_i (\mathbf{f}_i \cdot (\mathbf{v}_i - \langle\mathbf{v}\rangle) + \mathbf{l}_i \cdot \boldsymbol{\omega}_i), \tag{28}$$

describes the action of the particles on the gas turbulence. In this expression, it is considered that the average angular velocity of the gas flow is negligible compared to the angular velocity of a single particle, so that we avoid having to write the volume averaged angular momentum equation of the fluid phase.

Subtracting the mean kinetic energy equation and Eq. (27) from Eq. (23) results in the equation for the average gas temperature:

$$\frac{\partial}{\partial t}(\langle\rho\rangle c_\mathrm{v}\langle T\rangle) + \nabla\cdot(\langle\rho\rangle\langle\mathbf{v}\rangle c_\mathrm{v}\langle T\rangle) = -\nabla\cdot(\alpha_\mathrm{c}\{\mathbf{q}\}) + \alpha_\mathrm{c}\{\boldsymbol{\Sigma} : \nabla\mathbf{v}\}$$
$$- \nabla\cdot(\langle\rho\rangle c_\mathrm{v}\langle\mathbf{v}'T'\rangle) + \Pi_{\mathrm{eq}}, \tag{29}$$

where the term $\alpha_\mathrm{c}\{\boldsymbol{\Sigma} : \nabla\mathbf{v}\}$ describes the dissipation of mechanical energy.

To solve Eqs. (21)–(23), assumptions are required about the terms involving the gas fluctuating velocity, for example, about the tensor $\langle\rho\rangle\langle\mathbf{v}'\mathbf{v}'\rangle$ which is analogous to the Reynolds stress tensor in turbulent flows. Contrary to low-speed gas–particle flows, for which some models exist that have been applied successfully for pipe or channel flows (see e.g., Boulet and Moissette, 2002), there is unfortunately no available theory at present for turbulent supersonic gas–solid flows. Therefore, bearing in mind that (i) the flow of pure gas is considered below as laminar and (ii)

the particle volume fraction is low enough ($\alpha_p = 1 - \alpha_c \leqslant 3 \times 10^{-3}$), we assume that the particle volume concentration as well as the gas velocity and temperature fluctuations can be neglected in Eqs. (21)–(23): $\alpha_c \approx 1$, $k \approx 0$, $T' \approx 0$. In this case one can find from (27) that $\{\boldsymbol{\Sigma} : \nabla \mathbf{v}\} = \{\boldsymbol{\Sigma}\} : \nabla\langle \mathbf{v}\rangle + \Pi_k$, which means that the work of stresses on the particle surfaces, Π_k, is equal to the rate of additional dissipation of mechanical energy. Combining this relation and (29) we have

$$\frac{\partial}{\partial t}(\langle\rho\rangle c_v\langle T\rangle) + \nabla\cdot(\langle\rho\rangle\langle\mathbf{v}\rangle c_v\langle T\rangle) = -\nabla\cdot\{\mathbf{q}\} + \{\boldsymbol{\Sigma}\} : \nabla\langle\mathbf{v}\rangle + \Pi_k + \Pi_{eq}, \tag{30}$$

i.e. the work of stresses on the particle surfaces, which is always positive, increases the gas temperature. The averaged momentum and energy equations (22) and (23) simplify to

$$\frac{\partial}{\partial t}(\langle\rho\rangle\langle\mathbf{v}\rangle) + \nabla\cdot(\langle\rho\rangle\langle\mathbf{v}\rangle\langle\mathbf{v}\rangle) = \nabla\cdot\{\boldsymbol{\Sigma}\} + \Pi_m, \tag{31}$$

$$\frac{\partial}{\partial t}(\langle\rho\rangle\langle\mathbf{e}\rangle) + \nabla\cdot(\langle\rho\rangle\langle\mathbf{v}\rangle\langle e\rangle) = -\nabla\cdot\{\mathbf{q}\} + \nabla\cdot(\{\boldsymbol{\Sigma}\}\cdot\langle\mathbf{v}\rangle) + \Pi_{e\Sigma} + \Pi_{eq}. \tag{32}$$

In this case, the flow of the carrier gas is described by Eqs. (21), (31) and (32), where $\langle e\rangle$, $\langle\boldsymbol{\Sigma}\rangle$ and $\{\mathbf{q}\}$ are defined by the same relations (17) and (18) as in the pure gas. In addition to this simple model we estimated the possible turbulence generation by particles on the basis of Eqs. (21)–(23) and (27) (see Sections 2.6 and 4.3).

2.5. Boundary conditions

Fig. 1 shows a scheme of the computational domain for the plane cross-flow over the circular cylinder. Here the computational domain $ABCD$ is bounded by the entrance boundary AD, the plane of symmetry AB, the body surface BC and the exit boundary CD. Let $\mathbf{n}_b$ denote the unit vector normal to the boundary $ABCD$ and directed inside the computational domain.

2.5.1. Boundary conditions for the particulate phase

To formulate the boundary-value problem for Eq. (6) it is necessary to set the distribution function f at every point of the boundary $ABCD$. From analogy with the kinetic theory of gases (see e.g., Kogan, 1967), the boundary values of $f(\mathbf{r}_1, \mathbf{v}_1, \boldsymbol{\omega}_1, T_1, t)$ must be preset for the particles moving through the boundary into the domain, i.e. $\mathbf{v}_1\cdot\mathbf{n}_b > 0$. At the same time the values of $f(\mathbf{r}_1, \mathbf{v}_1, \boldsymbol{\omega}_1, T_1, t)$ for the particles moving through the boundary out of the domain are determined by the solution inside the domain.

Assuming that the entrance boundary AD of the computational domain is located in the free stream outside the shock layer, where the particles have the same parameters as the carrier gas, the following boundary condition can be assigned to AD:

$$f(\mathbf{r}, \mathbf{y}_1, t) = n_{p\infty}\delta_1(v_{1x} - V_\infty)\delta_1(v_{1y})\delta_1(v_{1z})\delta_3(\boldsymbol{\omega}_1)\delta_1(T_1 - T_\infty) \quad (\mathbf{v}_1\cdot\mathbf{n}_b > 0) \tag{33}$$

where V_∞, T_∞ and $n_{p\infty}$ are the gas velocity and temperature and the particle numerical concentration in the free stream; u_{1x}, u_{1y}, u_{1z} are the components of the particle velocity $\mathbf{v}_1$ in the coordinate system (x, y, z) (see Fig. 1), and δ_n is the n-variable Dirac function.

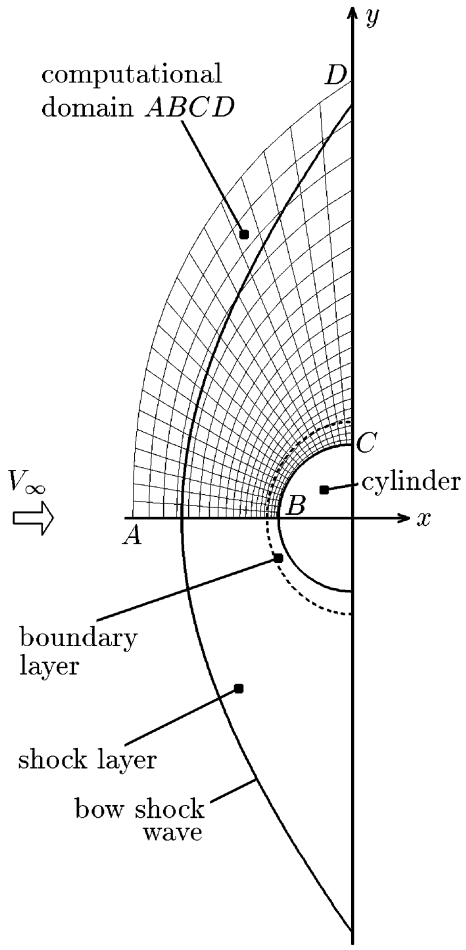

Fig. 1. Sketch of the flow structure, the computational domain *ABCD* and the grid.

At the exit boundary *CD* the average velocity of particles $\mathbf{u}_p$ is directed towards the outside of the domain. Since the mean square velocity c_p of the particle chaotic motion is much less here than $|\mathbf{u}_p|$, as was verified by the computations, the particles moving through this boundary towards the domain are much less numerous than the particles moving in the opposite direction. Therefore we can assume that there are no particles moving into the domain through the exit boundary *CD*: $f(\mathbf{r}, \mathbf{y}_1, t) = 0$ for $(\mathbf{v}_1 \cdot \mathbf{n}_b > 0)$.

At the plane of symmetry *AB* we use the ordinary symmetry condition extended to the case of a rotating particle: $f(\mathbf{r}, \mathbf{y}_1, t) = f(\mathbf{r}, \mathbf{y}_{1s}, t)$ for $(\mathbf{v}_1 \cdot \mathbf{n}_b > 0)$, where $\mathbf{v}_{1s} = \mathbf{v}_1 - 2\mathbf{n}_b(\mathbf{v}_1 \cdot \mathbf{n}_b)$, $\boldsymbol{\omega}_{1s} = \boldsymbol{\omega}_1 - 2\mathbf{n}_b \times (\boldsymbol{\omega}_1 \times \mathbf{n}_b)$.

At the body surface *BC* the distribution must satisfy the well-known kinetic boundary condition (see e.g., Kogan, 1967)

$$|\mathbf{v}_1 \cdot \mathbf{n}_w| f(\mathbf{r}_w, \mathbf{y}_1, t) = \int_{\mathbf{v}_1^- \cdot \mathbf{n}_w < 0} |\mathbf{v}_1^- \cdot \mathbf{n}_w| W_w(\mathbf{y}_1^- \to \mathbf{y}_1 | \mathbf{n}_w) f(\mathbf{r}_w, \mathbf{y}_1^-, t) \mathrm{d}\mathbf{y}_1^-, \tag{34}$$

where $\mathbf{v}_1 \cdot \mathbf{n}_w > 0$, $\mathbf{r}_w = R\mathbf{n}_w$, R is the cylinder radius, and $W_w(\mathbf{y}_1^- \to \mathbf{y}_1|\mathbf{n}_w)$ is the conditional distribution density of the particle parameters $\mathbf{y}_1$ after reflection from the surface for known values of the parameters before the collision, $\mathbf{y}_1^-$. The density $W_w(\mathbf{y}_1^- \to \mathbf{y}_1|\mathbf{n}_w)$ is to be calculated on the basis of the model of inelastic rebound of particles from the body surface. We neglect any surface roughness that can lead to stochastic dispersion of particles, therefore the particle parameters are being changed deterministically during the collision, according to the law $\mathbf{y}_1 = \mathbf{y}_w^+(\mathbf{y}_1^-, \mathbf{n}_w)$. In this case the density W_w takes the form $W_w(\mathbf{y}_1^- \to \mathbf{y}_1|\mathbf{n}_w) = \delta_7(\mathbf{y}_1 - \mathbf{y}_w^+(\mathbf{y}_1^-, \mathbf{n}_w))$.

2.5.2. The model of inelastic rebound of a particle from the body surface

We use the particle–wall collision model proposed by Tsirkunov et al., 1994a,b and extended by Volkov and Tsirkunov (2000) to the case of three-dimensional particle reflection from a surface with arbitrary orientation of the translational ($\mathbf{v}_1^-$) and rotational ($\boldsymbol{\omega}_1^-$) velocity vectors of the incident particle. The model is based on the experimental data by Lashkov (1991) about the restitution ratios of the normal and tangential velocities of the particle gravity center, a_{wn} and a_{wt}, which are assumed to obey the following relations obtained for initially non-rotating corundum particles and mild steel wall:

$$a_{wn} = 1 - \left(1 - \exp\left(-a_n|\mathbf{v}_1^-|^{b_n}\right)\right)\cos\varphi, \quad a_{wt} = a_t\varphi^6 + b_t\varphi^4 + c_t\varphi^2 + d_t, \tag{35}$$

where φ is the angle between the incident particle velocity vector $\mathbf{v}_1^-$ and the wall normal unit vector $\mathbf{n}_w$ ($\varphi < \pi/2$), and a_n, b_n, a_t, b_t, c_t, d_t are empirical coefficients. These relations are valid in a wide range of incident particle velocities: $50\ \mathrm{m/s} \leqslant |\mathbf{v}_1^-| \leqslant 500\ \mathrm{m/s}$.

The particle parameters before and after a collision are denoted herein after by the superscripts "−" and "+", respectively. We introduce the velocity vector at the particle–surface contact point $\mathbf{w}_1^- = \mathbf{v}_1^- - r_p\boldsymbol{\omega}_1^- \times \mathbf{n}_w$ and the local basis $(\mathbf{k}_w, \mathbf{n}_w, \mathbf{t}_w)$, where $\mathbf{k}_w = \mathbf{n}_w \times \mathbf{w}_1^-/|\mathbf{n}_w \times \mathbf{w}_1^-|$, $\mathbf{t}_w = \mathbf{k}_w \times \mathbf{n}_w$, and denote by subscripts the vector components in this basis. Then the components of particle velocities after collision can be calculated by the following relations:

$$v_{1k}^+ = v_{1k}^-, \quad \omega_{1n}^+ = \omega_{1n}^-, \quad \omega_{1t}^+ = \omega_{1t}^-, \quad T_1^+ = T_1^-, \quad v_{1n}^+ = -a_{wn}v_{1n}^-,$$

$$v_{lt}^+ = \begin{cases} a_{wt}v_{1t}^- - (1 - a_{wt})r_p\omega_{1k}^-, & \varphi > \varphi_*, \\ a_{wt}v_{1t}^- - (2/7)r_p\omega_{1k}^-, & \varphi \leqslant \varphi_*, \end{cases}$$

$$\omega_{1k}^+ = \begin{cases} \frac{5a_{wt}-3}{2}\omega_{1k}^- + \frac{5}{2}(a_{wt} - 1)\frac{v_{1t}^-}{r_p}, & \varphi > \varphi_*, \\ \frac{2}{7}\omega_{1k}^- - a_{wt}\frac{v_{1t}^-}{r_p}, & \varphi \leqslant \varphi_*, \end{cases}$$

where φ is the angle of incidence in the plane $(\mathbf{n}_w, \mathbf{t}_w)$, and φ_* is the root of the equation $a_{wt}(\varphi_*) = 5/7$ (for mild steel $\varphi_* = 79°, 5°$). Assuming that the thermal energy appeared in the process of impact is absorbed by the body surface and that the contact heat transfer can be neglected, the temperature as well as the internal energy of a particle do not change during the collision process, hence $e_w = [K_1]_w$.

2.5.3. Boundary conditions for the carrier gas

Here we set the boundary conditions needed to solve the equation of the carrier gas motion (21), (31) and (32). At the supersonic entrance boundary AD the gas flow was considered as

uniform with values of parameters given by $v_x = V_\infty$, $v_y = 0$, $\rho = \rho_\infty$, $T = T_\infty$. On the symmetry plane AB the symmetry conditions were laid down as follows: $v_y = \partial v_x/\partial y = \partial\rho/\partial y = \partial T/\partial y = 0$. At the body surface BC the conditions of impenetrability, absence of slip and equality of the gas and the given surface temperature T_w were set, i.e. $v_x = v_y = 0$, $T = T_w$.

The gas motion at the exit boundary CD outside of the thin subsonic boundary layer is supersonic under the conditions considered further. Therefore in the numerical solving of the viscous gas motion at the boundary CD, "soft" boundary conditions were used according to which disturbances in the vicinity of CD are assumed to be propagated only downstream. In practice the gas parameters $\tilde{\mathbf{A}} = (T, \rho, v_x, v_y)$ at the boundary CD were determined by linear extrapolation of the same parameters outwards the computational domain, i.e. the condition $\partial^2\tilde{\mathbf{A}}/\partial x^2 = 0$ was used.

2.6. The model of turbulence generation by particles

As described in Section 2.4, the carrier gas flow is computed assuming that velocity fluctuations are negligible. However, due to their inertia, particles exhibit very large relative velocities just behind the shock wave, therefore the particle Reynolds number in this region may be high enough for turbulence generation to be significant, due to the modification in velocity gradients associated with particle wakes. This is the reason why we aim here at assessing the level of turbulent kinetic energy arising from this phenomenon. To this purpose, Eq. (27) is rearranged to get the transport equation of the gas turbulent kinetic energy under the usual form:

$$\frac{\partial}{\partial t}(\langle\rho\rangle k) + \nabla\cdot(\langle\rho\rangle k) = D + P + \Pi_k - \langle\rho\rangle(\varepsilon + \varepsilon_g), \tag{36}$$

where $P = -\langle\rho\rangle\langle\mathbf{v}'\mathbf{v}'\rangle : \nabla\langle\mathbf{v}\rangle$ is the production term, $\langle\mathbf{v}'\mathbf{v}'\rangle = (2/3)k\mathbf{I} - 2\nu_t\langle\mathbf{S}\rangle$, and D is the diffusion term modeled in a standard way by $D = \nabla\cdot(\langle\rho\rangle\nu_k\nabla k)$, with $\nu_k = \nu + \nu_t/\sigma_k$, $\nu = \mu/\langle\rho\rangle$, $\nu_t = C_\mu k^2/\varepsilon$, $C_\mu = 0.09$, $\sigma_k = 1$. The turbulence-energy dissipation rate is expressed by the sum $\varepsilon + \varepsilon_g$, where the additional term ε_g is the so-called "dilatation dissipation", which is included to account for the compressibility effects, and is modeled by $\varepsilon_g = 2\varepsilon k/(\gamma\Re\langle T\rangle)$, following Sarkar and Balakrishnan (1990).

In order to estimate the gas turbulence level from (36), the turbulent kinetic energy source term Π_k is expressed according to Eq. (28). This "full" formulation, which is in agreement with the derivation by Crowe (2000) or Simonin and Squires (2001), has to be used here instead of the standard formulation (Elghobashi and Abou-Arab, 1983; Berlemont et al., 1990) which is known to be unable to predict any turbulence enhancement since the wake production is neglected. However, no rotational motion of particles was included in the earlier derivations, and the drag was assumed linear. Here, the particle rotation is taken into account, and we consider the more general case of non-linear drag force. Following Crowe (2000), the main part of the turbulence-energy dissipation rate, ε, in Eq. (36) is expressed by the algebraic relationship $\varepsilon = k^{3/2}/l_{mp}$, where l_{mp} is a hybrid length scale dependent on both an inherent integral length L of turbulence and the average inter-particle spacing $l_p = r_p\left(\sqrt[3]{\frac{4\pi}{3\alpha_p}} - 2\right)$. Kenning and Crowe (1997) defined the hybrid length scale by $l_{mp} = 2Ll_p/(L + l_p)$, which leads to an erroneous value when one of the two length scales tends to infinity. Later, Crowe (2000) defined the hybrid length scale by $l_{mp} = Ll_p/(L + l_p)$, an

expression leading to $l_{mp} = L/2$ for $l_p = L$, which is also incorrect. Therefore it was decided to use the simple formula $l_{mp} = \min(L, l_p)$, which does not suffer from the above mentioned drawbacks. Since we are dealing here with an initially laminar flow, there is no inherent length scale of turbulence, therefore we have to define L as a characteristic length scale of the dissipation due to the relative flow around a particle. For low particle Reynolds number Re_1, it is known that viscous effects are present up to the Oseen distance r_p/Re_1, while for higher Re_1, the characteristic length scale of viscous effects can be assumed of the order of the particle diameter $2r_p$. Thus we adopt the following expression for the length scale L:

$$L = 2r_p\left(1 + \frac{1}{Re_1}\right),$$

which meets the asymptotic requirements for small and large particle Reynolds number.

3. Method of computational simulation

The computation simulation of two-way coupled gas–particle flow with inter-particle collisions was based on the flow model described above. It represents a combination of a CFD-method for solving the governing equations for the carrier gas and the Direct Simulation Monte Carlo (DSMC) method for the particle phase. The detailed description of the whole algorithm is given in the paper by Volkov and Tsirkunov (2002). Here we only outline some important features of the computational procedure.

In the flow plane, two curvilinear grids, for continuous and dispersed phases, were introduced in the computational domain ABCD shown in Fig. 1. These grids are fitted to all boundaries of the calculation domain. The entrance boundary AD was placed outside the shock layer in the undisturbed flow. Both grids, for gas and particles, were strongly refined near the body contour to provide high accuracy inside the boundary layer at high Reynolds number Re_∞. The computational grid for the gas phase contained 60 cells along the cylinder surface and 240 cells in the direction normal to the surface. From 30 to 50 cells in the normal direction were located inside the boundary layer. Depending on the particle radius, the grid used for simulation of the dispersed phase flow contained from 60 to 120 cells along the surface and from 120 to 240 cells in the normal direction.

In the numerical algorithm, the dispersed phase was represented as a set of a large number of simulated particles. The motion and heating of these particles, controlled by the gas–particle interaction and the particle–particle collisions, were computed using the DSMC method based on the kinetic model described in Section 2.2. This method is widely used in rarefied gas dynamics (see, e.g., Bird, 1994). Simulation of the particle behavior during a time step Δt was splitted into the stage of collisions between particles in every grid cell and the stage of motion and heating. The inter-particle collisions were considered as random events and the majorant frequency scheme (Ivanov and Rogazinsky, 1988) modified by Volkov and Tsirkunov (1996) was used for their simulation. The motion and heating of the ith particle between collisions were considered as deterministic processes, described by the momentum, angular momentum and energy equations written along the particle trajectory, together with the kinematic relation for the particle's position vector

$$\frac{\mathrm{d}\mathbf{v}_i}{\mathrm{d}t}=\frac{\mathbf{f}_i}{m_\mathrm{p}},\quad \frac{\mathrm{d}\boldsymbol{\omega}_i}{\mathrm{d}t}=\frac{\mathbf{l}_i}{I_\mathrm{p}},\quad \frac{\mathrm{d}T_i}{\mathrm{d}t}=\frac{q_i}{m_\mathrm{p}c_\mathrm{p}^\circ},\quad \frac{\mathrm{d}\mathbf{r}_i}{\mathrm{d}t}=\mathbf{v}_i.$$

These equations are consistent with the left part of the kinetic equation (6). The current fields of macroparameters of the dispersed phase defined by (8) were obtained as the averaged values of parameters of the simulated particles over every cell of the grid. The same procedure was used to calculate the macroparameters at the body surface defined by (9). The average number of simulated particles in the computational domain was approximately 1.5×10^6.

The modified Navier–Stokes equations were numerically integrated over a time step Δt using a finite-volume scheme. Eqs. (21), (31) and (32) were written in the so-called generalized coordinates in which the computational grid shown in Fig. 1 was orthogonal and uniform. At first, the TVD-scheme by Harten (see Yee and Harten, 1987) was applied to solve the inviscid part of the carrier gas equations. Then explicit central finite-difference approximations were used to calculate the contribution of the "viscous" terms. The gas–particle interaction terms $\mathbf{\Pi}_m$, $\Pi_{e\Sigma}$, and Π_eq, were fixed during Δt.

The time step Δt was selected to satisfy the following three conditions: (1) the convergence condition of the finite-volume scheme for the Navier–Stokes equations; (2) Δt must be less than the average local particle free time between collisions and (3) it must be less than the average time of particle motion across any cell of the computational grid.

Steady-state flow fields of the dispersed phase and the carrier gas were obtained as the limit of a time-depending solution at large t. In doing so the macroparameters of the dispersed phase were obtained by time-averaging the grid cell-averaged parameters of simulated particles over a long time interval (over several hundred time steps Δt).

4. Computational results and discussion

4.1. Governing parameters

The solution of the boundary-value problem for Eqs. (6), (21), (31) and (32) with the given boundary conditions and additional relations (1)–(4), (7), (10)–(12), (17), (18), (24) and (25) depends on 26 parameters, among them 24 were fixed while two ones, the particle radius r_p, and the free stream particle volume fraction $\alpha_{\mathrm{p}\infty}$, were varied.

In the computational simulation, the carrier gas was air, the particle material was synthetic corundum, the material of the cylinder was mild steel. The flow parameters and the body size were similar to those in experiments performed in a supersonic wind tunnel in TsAGI (Vasilevskii et al., 2001). Values of all governing parameters are given in Table 1. The empirical constants a_c, b_c, c_c, d_c in Eq. (3) and a_n, b_n, a_t, b_t, c_t, d_t in Eq. (35) were determined from the experimental data. The restitution coefficients a_rn and a_rt in the particle–particle collision model cannot be determined with reasonable accuracy nowadays neither from experiments nor theoretically, therefore their values were taken from physical considerations. In Table 1, $T_0=T_\infty(1+(\gamma-1)M_\infty^2/2)$ is the adiabatic stagnation temperature.

The carrier gas flow parameters correspond to the Mach number $M_\infty=2$ and the Reynolds number $Re_\infty=2R\rho_\infty V_\infty/\mu_\infty=10^5$. The lower bound of the particle radius ($r_\mathrm{p}=0.2$ μm) corre-

Table 1
Input data for calculations

Parameter	Numerical value
γ	1.4
$\mathscr{R}$ (J/(kg K))	286.9
Pr	0.76
μ_s (kg/ms)	1.71×10^{-5}
T_s (K)	273
C_s (K)	117
V_∞ (m/s)	494.5
ρ_∞ (kg/m^3)	0.104
T_∞ (K)	151.7
$R[m]$	0.01
T_w/T_0	0.5
ρ_p° (kg/m^3)	3950
a_c (J/(kg K^4))	3.04×10^{-6}
b_c (J/(kg K^3))	-7.01×10^3
c_c (J/(kg K^2))	5.54
d_c (J/(kg K))	-341.8
a_{rn}	0.5
a_{rt}	0.9
b_n	0.61
$a_n[(s/m)^{b_n}]$	0.1
a_t	0.0219
b_t	0.114
c_t	-0.288
d_t	0.69
r_p (μm)	0.2, . . . , 10
$\alpha_{p\infty}$	$10^{-6}, \ldots, 3 \times 10^{-5}$

sponds to very fine particles and the upper bound ($r_p = 10$ μm) to coarse-grained ones. Accordingly, the "formal" particle Stokes number $St_\infty = 2\rho_p^\circ r_p^2 V_\infty/(9\mu_\infty R)$ lies in the range $0.168 \leqslant St_\infty \leqslant 420$. For the values of $\alpha_{p\infty}$ in Table 1, the particle mass concentration C_∞, defined as the ratio of the bulk density of the dispersed phase to the mixture density, varies from 3.6% to 53%. Most of the computational results were obtained for the following four cases: smallest concentration, largest concentration and also for $\alpha_{p\infty} = 3 \times 10^{-6}$ ($C_\infty = 10\%$) and $\alpha_{p\infty} = 10^{-5}$ ($C_\infty = 27.5\%$).

4.2. Particle flow structure

Particle phase flow patterns were found to be quite different for fine particles with radius smaller than the critical value r_{p*} and for larger particles. All other parameters being fixed, the critical radius depends on $\alpha_{p\infty}$ because the carrier gas flow field is affected by $\alpha_{p\infty}$ due to the reverse effect from the dispersed phase. However this dependence is weak, e.g., $r_{p*} \approx 0.283$ μm for $\alpha_{p\infty} \to 0$, $r_{p*} \approx 0.3$ μm for $\alpha_{p\infty} = 3 \times 10^{-6}$, $r_{p*} \approx 0.35$ μm for $\alpha_{p\infty} = 10^{-5}$. The role of inter-particle collisions is negligible for fine particles, whereas the effect of collisions on the behavior of larger particles increases with increasing $\alpha_{p\infty}$ and becomes essential even at very low particle volume

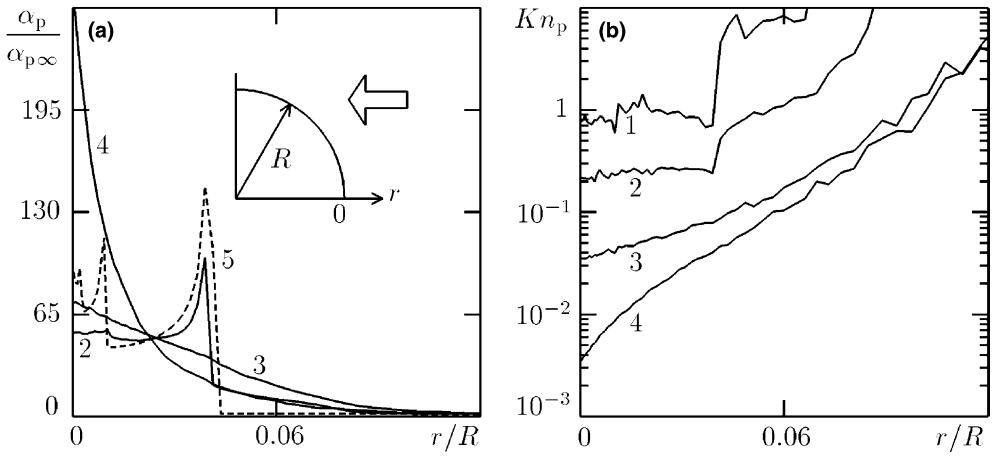

Fig. 2. Distribution of (a) relative particle volume fraction $\tilde{\alpha}_p = \alpha_p/\alpha_{p\infty}$ and (b) local Knudsen number Kn_p in the "gas" of particles along the stagnation streamline. $r_p = 1$ μm. Curve 1, $\alpha_{p\infty} = 10^{-6}$; 2, $\alpha_{p\infty} = 3\times10^{-6}$; 3, 5, $\alpha_{p\infty} = 10^{-5}$; 4, $\alpha_{p\infty} = 3\times10^{-5}$. The dashed curve 5 was obtained without collisions between particles.

fraction in the free stream, as illustrated by Fig. 2. The distribution of the relative particle volume fraction $\alpha_p/\alpha_{p\infty}$ along the stagnation streamline is modified qualitatively when $\alpha_{p\infty}$ increases from 10^{-6} to 3×10^{-5} (see Fig. 2(a)). At lower $\alpha_{p\infty}$, the distribution is very close to that for collisionless particle phase flow ($\alpha_{p\infty}\to 0$), as shown by the dashed curve 5. In this limiting case, it is known that singular surfaces appear in the flow of the particle phase over a blunt body (Tsirkunov et al., 2002). These surfaces are the envelopes of trajectories of particles reflected from the body surface. Theoretically, the particle concentration on these envelopes tends to infinity, however in the computational simulations we have only sharp peaks. The envelopes of trajectories after the first and second reflections of particles from the body are labeled *AA* and *BB* in Fig. 3(a), respectively. The sharp peaks on the dashed line 5 in Fig. 2(a) correspond to the location of these envelopes at the stagnation streamline. At higher $\alpha_{p\infty}$, the particle volume fraction increases monotonically towards the body surface, as shown by curves 3 and 4 in Fig. 2(a). It is seen that the chaotically moving particles can penetrate upstream a double distance compared with that of the reflected particles moving regularly without collisions (compare curves 3 and 5). Note that increasing the free stream particle concentration or increasing the particle radius results in the same effect. Our calculations showed that the chaotically moving particles of radius $r_p = 10$ μm leave the shock layer and enter the area of undisturbed flow in front of the bow shock wave.

An important parameter characterizing the role of inter-particle collisions is the local Knudsen number in the "gas" of particles, Kn_p, which is defined by

$$Kn_p = \frac{\lambda_p}{R}, \quad \lambda_p = \frac{n_p}{2\nu_p}\sqrt{[v_1^2]_1}. \tag{37}$$

Here λ_p is the mean free path of dispersed particles between collisions with each other, ν_p is the frequency of inter-particle collisions in a unit volume of gas–particle mixture. The distribution of Kn_p along the stagnation streamline in the shock layer is shown in Fig. 2(b). It is seen that the local Knudsen number and, hence, the mean free path of particles can vary within very wide limits (a hundred times and more) across the near-wall layer of chaotically moving and colliding

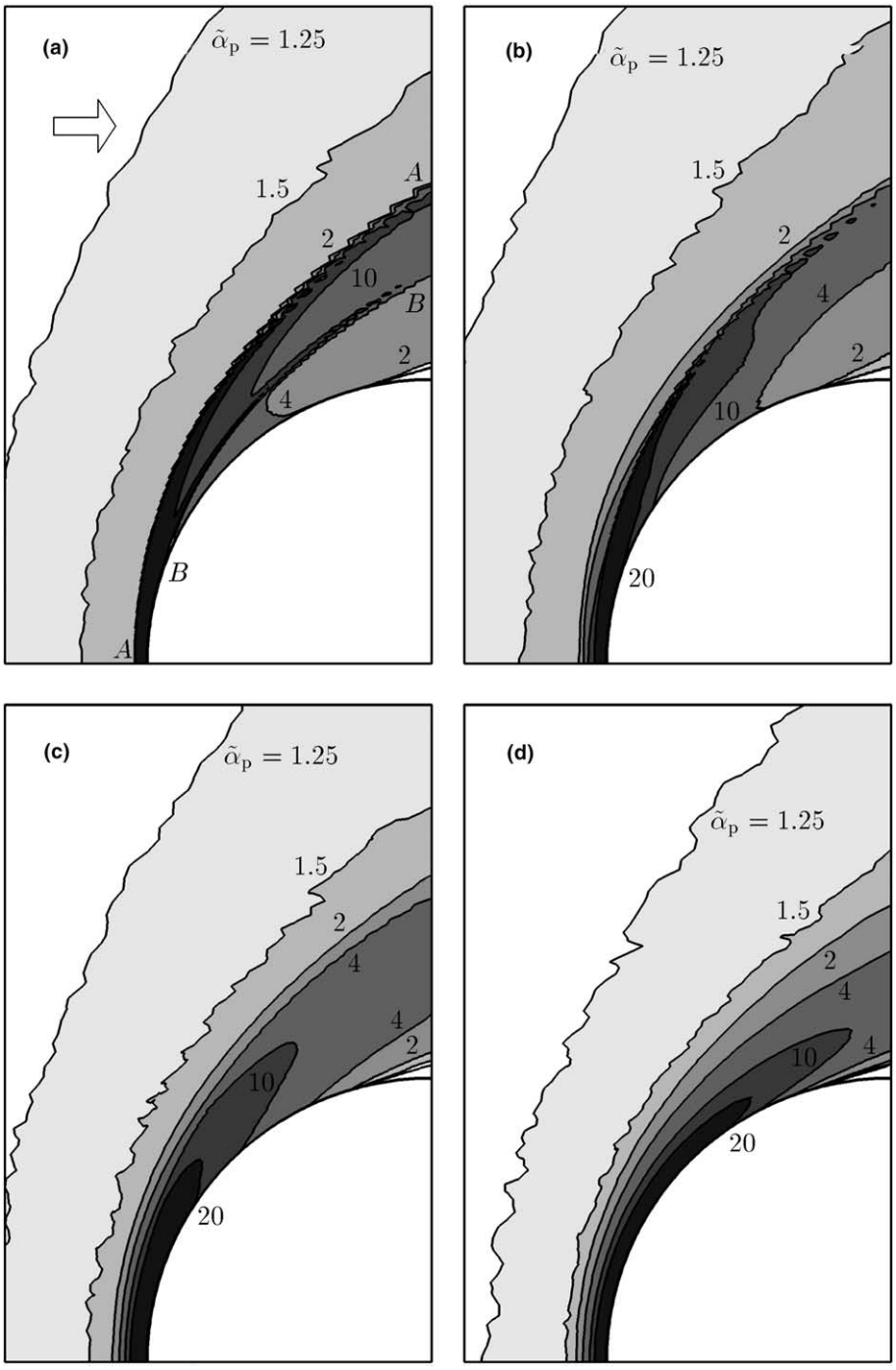

Fig. 3. Contours of constant relative particle volume fraction $\tilde{\alpha}_p = \alpha_p/\alpha_{p\infty}$. $r_p = 1$ μm. (a) Without collisions between particles, (b)–(d) with collisions. (a), (c) $\alpha_{p\infty} = 10^{-5}$; (b) $\alpha_{p\infty} = 3 \times 10^{-6}$; (d) $\alpha_{p\infty} = 3 \times 10^{-5}$.

particles. In those cases that the inter-particle collisions are essential in the flow, the local Knudsen number decreases monotonically towards the body and has a minimum at the stagnation point (see curves 3 and 4 in Fig. 2(b)). This means that the collision frequency reaches the highest value near the stagnation point.

Fig. 3 illustrates the influence of collisions between particles ($r_p = 1$ μm) on the particle concentration field in the shock layer. Fields (b)–(d) in this figure were computed with taking inter-particle collisions into account. For comparison, field (a) was calculated at $\alpha_{p\infty} = 10^{-5}$ without collisions, but with taking into account the reverse action of particles on the carrier gas flow. Due to particle–particle collisions, the singular surfaces labeled AA and BB in the particle concentration field (a) disappear. As the particle volume fraction increases, the singularity BB first disappears for $\alpha_{p\infty} = 3 \times 10^{-6}$, and then the singularity AA also disappears (at $\alpha_{p\infty} = 10^{-5}$). As the layer of colliding particles moves downstream, it is separated from the cylinder surface. Curves 3 and 4 in Fig. 2(a) show that the relative particle concentration in this layer increases with $\alpha_{p\infty}$, and the thickness of this layer decreases as can be seen from comparison between fields (c) and (d).

Calculations of the particle concentration fields were carried out also for fine particles ($r_p = 0.3$ μm), for particles with radius slightly higher than the critical one ($r_p = 0.5$ μm) and for large particles ($r_p = 2$ μm and 3 μm). The fields for $r_p = 0.5$ μm and $r_p = 2$ μm inside the whole shock layer are shown in Fig. 4. The detailed structure of the particle concentration field inside the cylinder boundary layer is presented in Fig. 5 for particles with $r_p = 0.3$ μm, 0.5 μm and 1 μm.

Fine particles move practically without collisions and, hence, both the collisional and collisionless particle phase flow models yield very close results everywhere, see (a) and (b) in Fig. 5. Moreover, comparison of fields (a) and (c) in Fig. 4 and (c) and (d) in Fig. 5 shows that the concentration patterns of particles with radius even slightly larger than r_{p*}, calculated with and without collisions, are also very close everywhere except in the boundary layer. In contrast, for coarse-grained particles ($r_p > 1$ μm) the collisions modify the particle phase flow field very strongly everywhere (compare patterns (b) and (d) in Fig. 4, and also (e) and (f) in Fig. 5).

In the model of gas–particle interaction (see Section 2.3) the effects of inertia, compressibility and rarefaction in the flow over a particle were taken into account. To clarify the role of these effects, which are characterized by the particle Reynolds number Re_1, Mach number M_1, and Knudsen number Kn_1, respectively, we kept track of values of Re_1, M_1 and Kn_1 for every particle moving in the shock layer. The Knudsen number Kn_1 is defined by $Kn_1 = \lambda_g/r_p$, where $\lambda_g = 1.255\mu/(\rho\sqrt{\Re T})$ is the free path of molecules near a particle (see, e.g., Kogan, 1967). The results for incident particles moving near the stagnation streamline are discussed below.

For particles of radius $r_p \leqslant 1$ μm the Reynolds number does not exceed 40. For larger particles (1 μm $< r_p \leqslant 3$ μm) the value of Re_1 outside the boundary layer does not exceed 60, whereas inside the boundary layer it ranges up to 180 for particles of radius $r_p = 3$ μm when they reach the cylinder surface. The latter effect is caused by an increase in gas density and a decrease in gas temperature and, hence, in viscosity coefficient μ, inside the boundary layer towards the "cold" surface. As it follows from these data, the inertial effects can be very essential in the shock layer. It is well known that an unsteady separated flow with a large-scale vortex structure in the wake behind a spherical particle arises if $Re_1 \geqslant 200$. At lower Reynolds number, a separated bubble of restricted volume is attached to the back part of the particle. This bubble disappears and a non-separated flow is observed at $Re_1 \leqslant 5$. Thus, for the considered flow parameters, particles move inside the shock layer with attached separated bubbles or without flow separation.

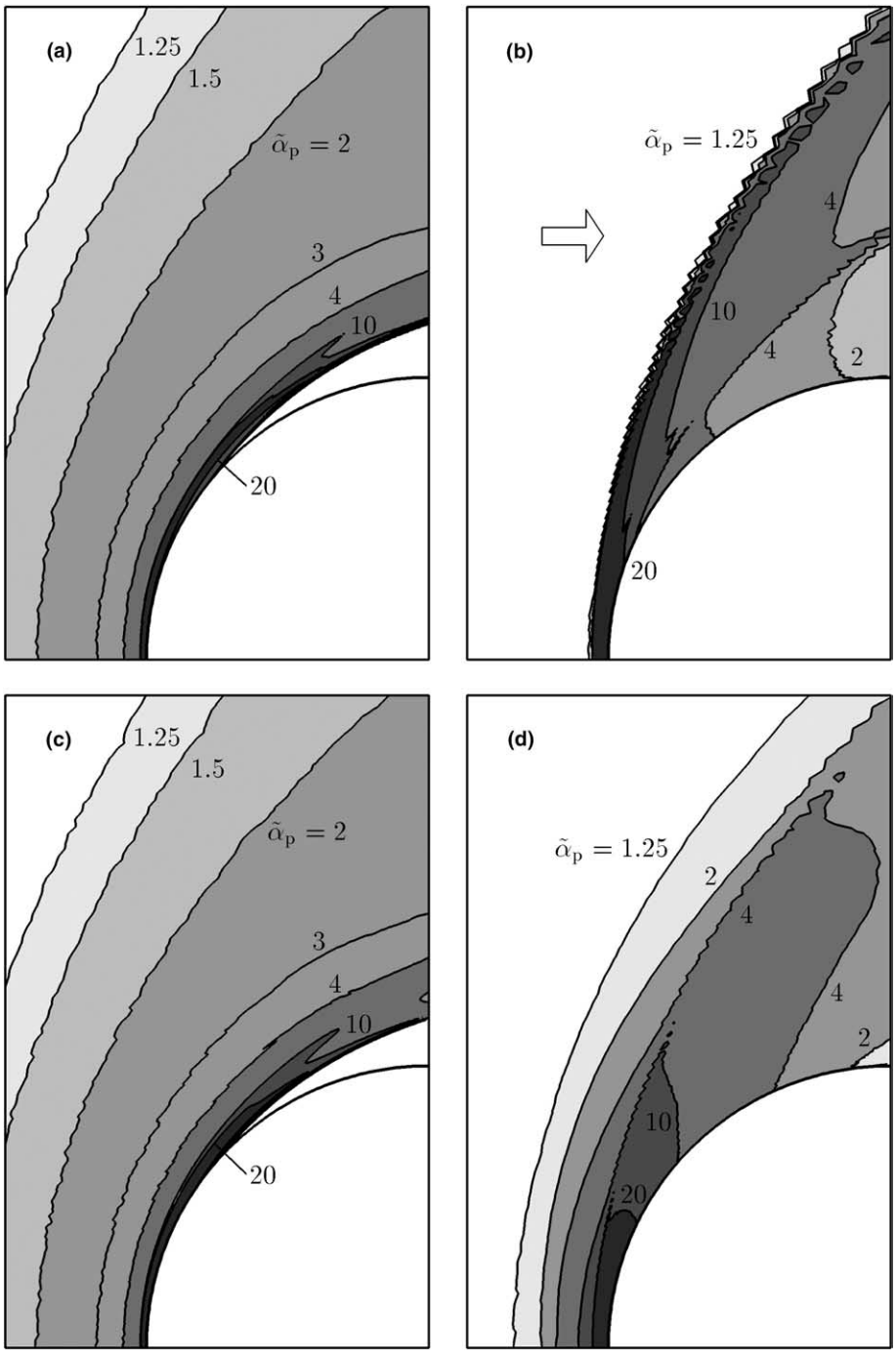

Fig. 4. Contours of constant relative particle volume fraction $\tilde{\alpha}_p = \alpha_p/\alpha_{p\infty}$. (a), (c) $r_p = 0.5$ μm; (b), (d) $r_p = 2$ μm. $\alpha_{p\infty} = 10^{-5}$; (a), (b) without collisions between particles, (c), (d) with collisions.

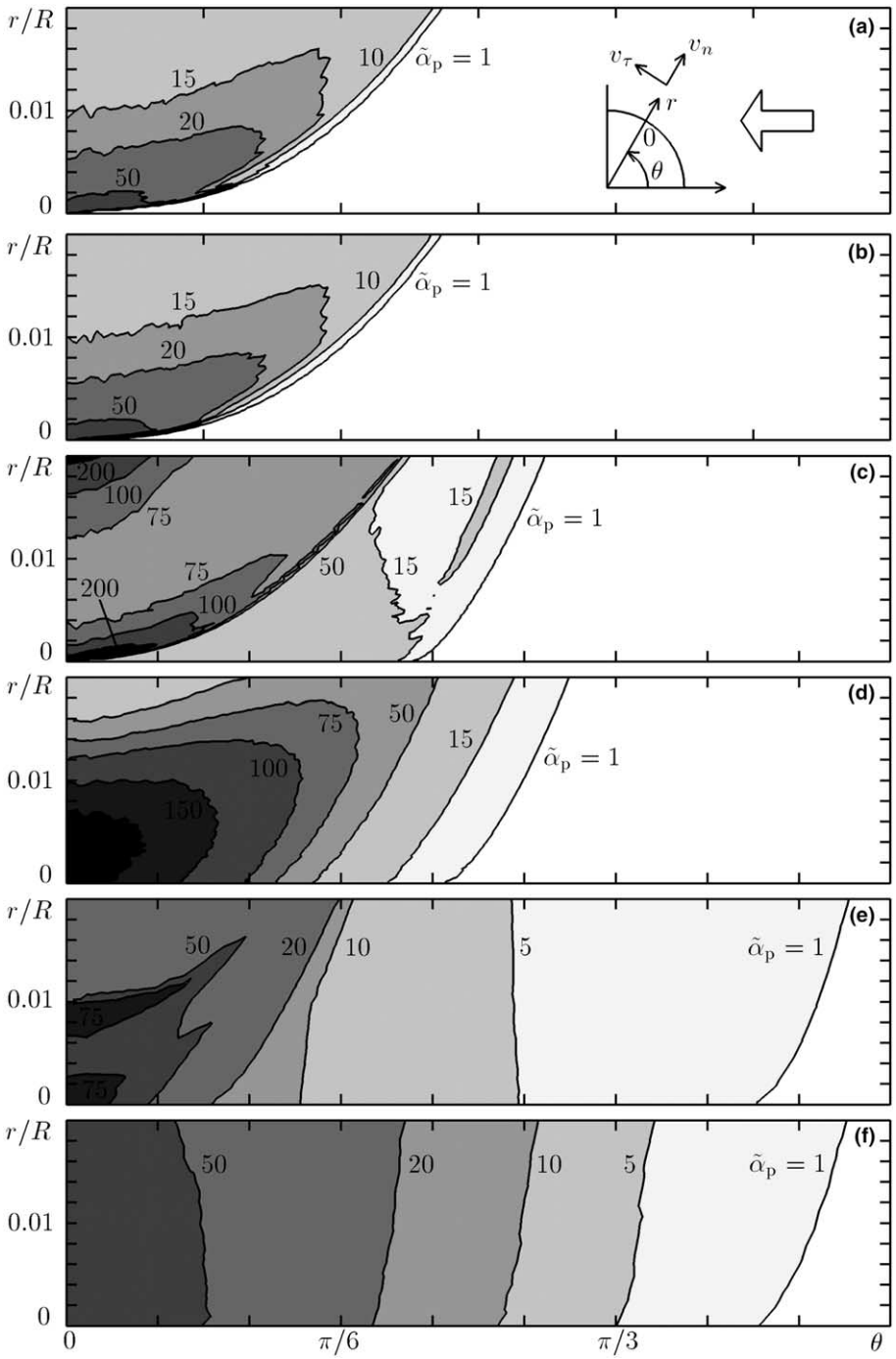

Fig. 5. Contours of constant relative particle volume fraction $\tilde{\alpha}_p = \alpha_p/\alpha_{p\infty}$ inside the boundary layer. The angular location θ is measured from the stagnation point as shown in (a). $\alpha_{p\infty} = 10^{-5}$. (a), (c), (e) without collisions between particles, (b), (d), (f) with collisions. (a), (b), $r_p = 0.3$ μm; (c), (d), $r_p = 0.5$ μm; (e), (f) $r_p = 1$ μm.

Particles of all sizes entering the shock layer have a high subsonic relative velocity just behind the bow shock wave. As particles move towards the cylinder surface, the Mach number M_1 can increase, decrease, or vary non-monotonically. For large particles ($r_p \geqslant 3$ μm), M_1 increases, for fine particles ($r_p \leqslant 0.3$ μm) M_1 decreases. In the intermediate range of r_p, M_1 first decreases and then increases due to the decrease in sound speed in the boundary layer on the "cold" wall. Thus the effect of compressibility on the gas–particle interaction can therefore be very important.

The Knudsen number Kn_1 of a particle moving from the shock wave to the body is weakly decreasing. For fine particles, the flow regime is transitional, e.g., Kn_1 is of order 1 for $r_p = 0.3$ μm, where as with increasing r_p the regime becomes first slipping (e.g., Kn_1 of order 0.1 for $r_p = 3$ μm) and then close to continuum. Therefore, the rarefaction effects are important and must be taken into account.

The kinetic model described in Section 2.2 and the DSMC technique used for the simulation of collisions between particles are based, among others, on the assumption that the mean free path of particles λ_p is much less than the momentum response length λ_d. The relation between these lengths was a subject of special study in our calculations.

Consider the particle momentum and thermal response lengths λ_d and λ_t, defined as the distances at which the relative particle velocity and the difference between gas and particle temperatures decrease by a factor $e = 2.718\ldots$ More exactly, λ_d and λ_t are determined in every flow point from the Cauchy problem for a particle moving in a stagnant gas with initial velocity and temperature equal to the instantaneous values of the relative velocity and temperature at the given point. Such momentum and thermal response distances were calculated at the axis of symmetry directly behind the bow shock, and the results are shown by the solid curves in Fig. 6(a). For comparison, λ_d and λ_t were calculated for the Stokes flow over a particle ($CD = 24/Re_1$ and $Nu_p = 2$), an approximation widely used for estimates, and the results are presented in the same figure (see dashed curves). For the given flow parameters and particles, we have

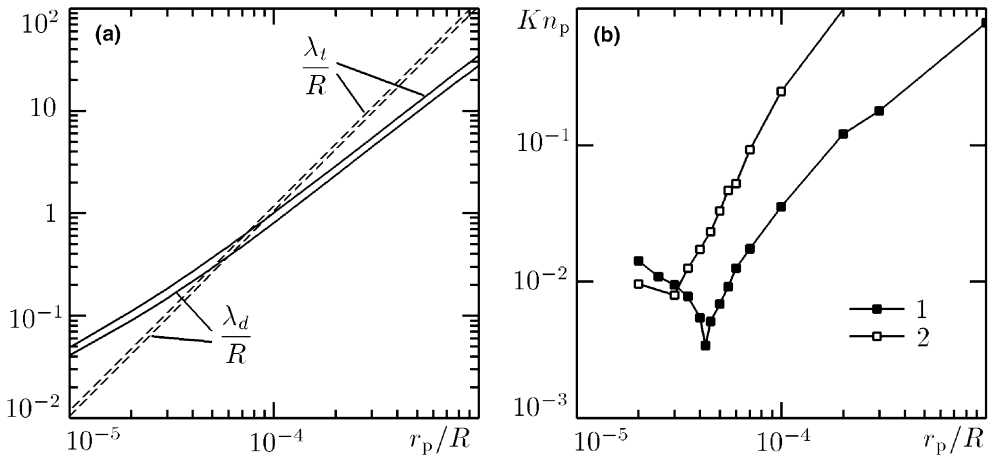

Fig. 6. (a) Dynamic (λ_d) and thermal (λ_t) relaxation lengths of particles just behind the bow shock on the stagnation streamline versus particle radius r_p: solid curves correspond to CD, given by Henderson correlations and Nu_p by formula (13); dashed curves correspond to the Stokes' law $CD = 24/Re_1$ and $Nu_p = 2$. (b) Local Knudsen number Kn_p at the stagnation point versus particle radius r_p: curve 1, $\alpha_{p\infty} = 10^{-5}$; 2, $\alpha_{p\infty} = 3 \times 10^{-6}$.

$\lambda_t > \lambda_d$ and $\lambda_t/\lambda_d \approx$ const. The solid curve for λ_d can be approximated by the power function $\lambda_d/R \sim (r_p/R)^{3/2}$, whereas the dashed curve corresponding to the Stokes flow is better represented by $\lambda_d/R \sim (r_p/R)^2$. The Stokes flow model can be observed to yield underestimated values of λ_d and λ_t for small particles and overestimated ones for large particles.

As it follows from Fig. 2(b), the most significant effect of inter-particle collisions takes place in the stagnation region. The smallest value of the local Knudsen number Kn_p is obtained at the stagnation point. The dependence of this value on the particle radius, all other parameters being fixed, is plotted in Fig. 6(b). For $r_p \geqslant r_{p*}$ Kn_p decreases with decreasing r_p. Such a behavior can be explained by an estimation of λ_p derived from the elementary kinetic theory. In fact, we have $v_p \sim n_p^2 r_p^2 \sqrt{[(\mathbf{v}_1 - \mathbf{u}_p)^2]_1}$, where $\mathbf{u}_p$ is the macroscopic velocity of the dispersed phase. Substituting this expression into Eq. (37) and using the estimate $\alpha_p \sim n_p r_p^3$ we obtain

$$Kn_p \sim \frac{1}{\alpha_{p\infty}} \frac{r_p/R}{\alpha_p/\alpha_{p\infty}} \sqrt{\frac{[\mathbf{v}_1^2]_1}{[(\mathbf{v}_1 - \mathbf{u}_p)^2]_1}}.$$

As it follows from the numerical results, the particle volume fraction α_p at the stagnation point increases with decreasing particle radius r_p (for $r_p \geqslant r_{p*}$), and, hence, the Knudsen number decreases according to the last formula.

If $r_p \leqslant r_{p*}$, then Kn_p increases with decreasing r_p. In the latter case, we have fine particles, and, theoretically, collisions between them cannot occur. However, in the DSMC technique, collisions between particles located in the same grid cell can formally occur if these particles have unequal velocities. Such a situation takes place in the cell adjacent to the stagnation point for fine particles which change their direction of motion from nearly normal to the wall to tangential. Another reason for the collisions between fine particles in the mentioned cell is that the particle gravity center cannot near the body surface closer than the particle radius r_p. At this distance even particles with $r_p \leqslant r_{p*}$ have a non-zero wall normal velocity, therefore they can rebound from the body at the stagnation point, resulting also in that the particles in the adjacent grid cell have unequal velocities and can collide. An investigation carried out to estimate the influence of this simulation effect on the computational results showed that such formal collisions between fine particles in the cell near the stagnation point practically do not influence the fields of all other macroparameters of both phases because the area where the frequency of collisions is not negligible is restricted, in fact, by a single near-wall cell.

Comparison of Kn_p with λ_d/R for equal particle radii showed that in the range $\alpha_{p\infty} \geqslant 3 \times 10^{-6}$ the momentum response length λ_d is several times larger than the particle mean free path λ_p and, hence, the fundamental assumption accepted for the derivation of the kinetic equation (6) is valid.

4.3. Influence of particles on the carrier gas flow

Here we consider the question of how the particle phase modifies the gas flow field in the shock layer. Fig. 7 illustrates such a modification by an example of the field of the local Mach number $M = |\mathbf{v}|/\sqrt{\gamma \Re T}$. The fields (a)–(d) in this figure are obtained for the same governing parameters as the fields (a)–(d) in Fig. 3. The field (b) in Fig. 7 corresponding to $\alpha_{p\infty} = 3 \times 10^{-6}$ is very close to the one calculated for the pure gas flow, however one can see slight distortions of the Mach number contours near the body surface. This means that the reverse action of the particles begin to play

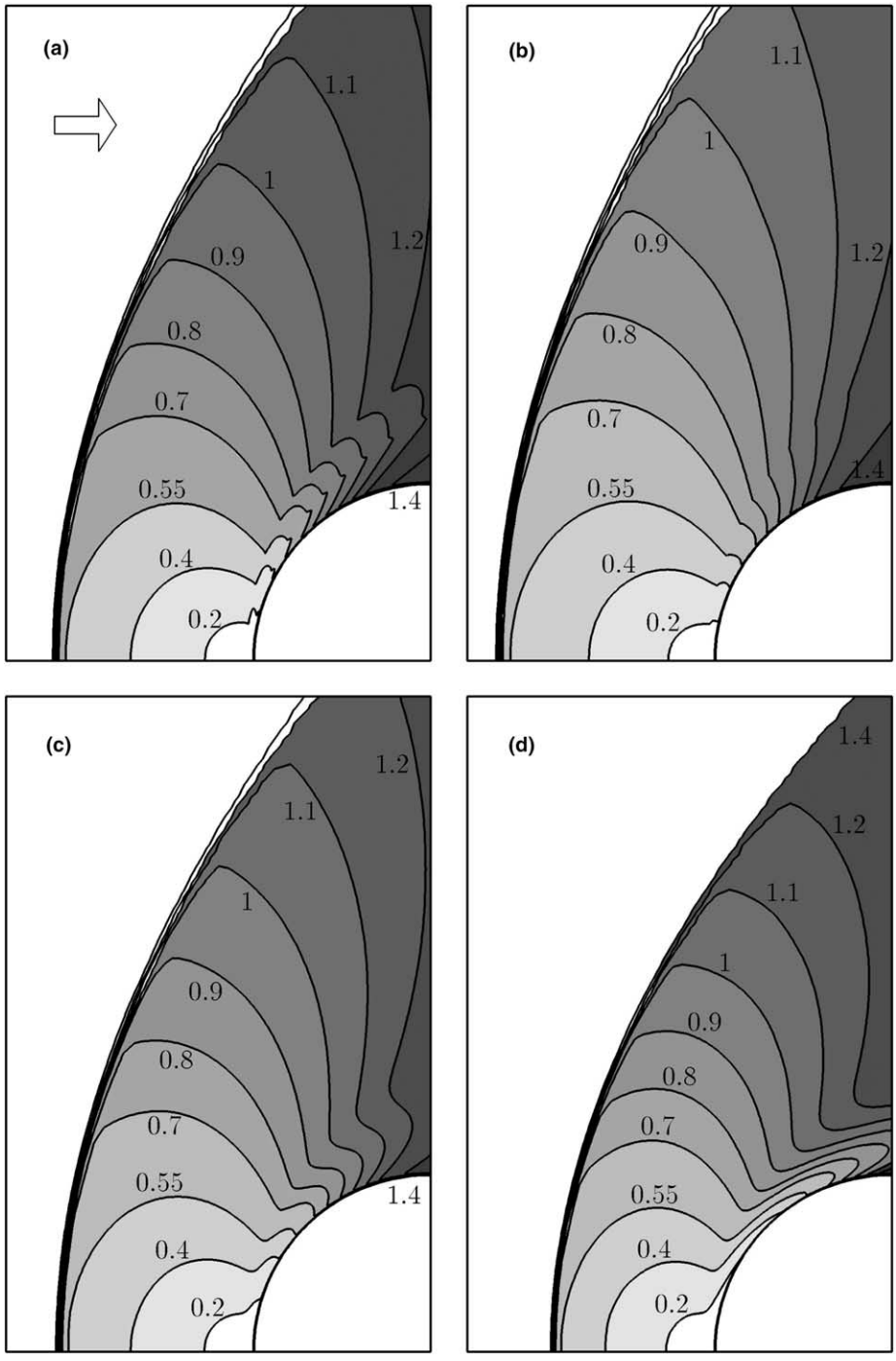

Fig. 7. Contours of constant local Mach number $M = |\mathbf{v}|/\sqrt{\gamma \Re T} \cdot r_p = 1$ μm. (a) Without collisions between particles, (b)–(d) with collisions. (a), (c) $\alpha_{p\infty} = 10^{-5}$; (b) $\alpha_{p\infty} = 3 \times 10^{-6}$; (d) $\alpha_{p\infty} = 3 \times 10^{-5}$.

a noticeable role in the flow at $\alpha_{p\infty} \approx 3 \times 10^{-6}$, the particle size and other governing parameters being fixed. As it follows from Fig. 2(a), the inter-particle collisions begin to play a noticeable role just at the same $\alpha_{p\infty}$. Moreover, analysis of the numerical results shows that the same situation takes place for particle sizes in the range $r_{p*} < r_p \lesssim 1$ μm. For particles of these sizes the Stokes number is of order of unity or less ($St_\infty = 4.2$ in Figs. 3 and 7). Therefore, for particles whose radius slightly exceeds the critical one, both effects, i.e. collisions between particles and reverse action of the dispersed phase on the gas flow, come into play at the same particle concentration $\alpha_{p\infty}$ and, hence, these effects must be taken into account in the two-phase flow model simultaneously. The situation is quite different for particles of considerably larger radius ($r_p \gtrsim 3$ μm): in this case, inter-particle collisions come into play at concentration $\alpha_{p\infty}$ about 10 times smaller than the concentration for which significant two-way coupling effects begin to take place. Note that estimations of the maximum concentration of coarse-grained particles for the effects of collisions and reverse action to be negligible were obtained by Tsirkunov (1993, 2001).

As can be seen by comparing the fields (b), (c) and (d) in Fig. 7, increasing $\alpha_{p\infty}$ results in a decrease of the distance between the shock wave and the cylinder surface. Inside the near-wall layer, particles move along the body surface slowly due to their inelastic and frictional collisions with the body surface or with other particles. As can be seen, particles slow down the gas flow in this layer. For example, in the case $\alpha_{p\infty} = 3 \times 10^{-5}$ the gas flow inside this layer remains fully subsonic up to the middle cross-section of the cylinder, i.e. up to $\theta = 90°$, whereas the pure gas flow becomes supersonic downstream from $\theta \approx 50°$ (the angle θ is defined in Fig. 5(a)).

The fields of local Mach number shown in Fig. 7(a) and (c), were obtained at $\alpha_{p\infty} = 10^{-5}$ without and with inter-particle collisions, respectively. The fractures in the Mach number contours in Fig. 7(a) match the locations of the envelopes of the reflected particle's trajectories in the collisionless flow. The relative particle concentration $\alpha_p/\alpha_{p\infty}$ at these envelopes becomes infinite. Collisions between particles make these particle concentration singularities disappear and, hence, leads to smoother gas flow field.

The effect of the dispersed phase on the gas flow inside the cylinder boundary layer is illustrated by Fig. 8. The profiles of the tangential gas velocity v_τ are shown in three cross-sections specified by $\theta = \text{const}$. Thin curves are for the pure gas flow, while thick and dashed curves correspond to the carrier gas flow with and without inter-particle collisions, respectively. The particle radius in this figure is slightly higher than the critical one. The fracture of the dashed curve 1 corresponds to the upper bound of the layer of reflected particles in this cross-section. The distance between this bound and the body surface is about three times as large as the boundary layer thickness in the pure gas flow. In the region where the reflected particles are present, the distribution of v_τ in the two-phase flow significantly differs from that in the pure gas flow. As shown by the thick and dashed curves 2 and 3, the profiles of the tangential velocity v_τ downstream from the stagnation point in the two-phase flow do not tend to those in the pure gas flow . This means that the particles of near-critical radius significantly modify the velocity field of the carrier gas not only inside the boundary layer but also in a much larger region of the flow near the surface. Numerical results for particles of radius $r_p < r_{p*}$ show that even very fine particles modify the carrier gas flow far outside the boundary layer. This result allows us to conclude that the hypothesis that fine particles do not affect the gas flow outside the boundary layer, an assumption used by Osiptsov (1985), is not true.

The comparison between the thick and dashed curves 1 and 2 in Fig. 8 shows that the distribution of v_τ inside the boundary layer is qualitatively modified by the inter-particle collisions at

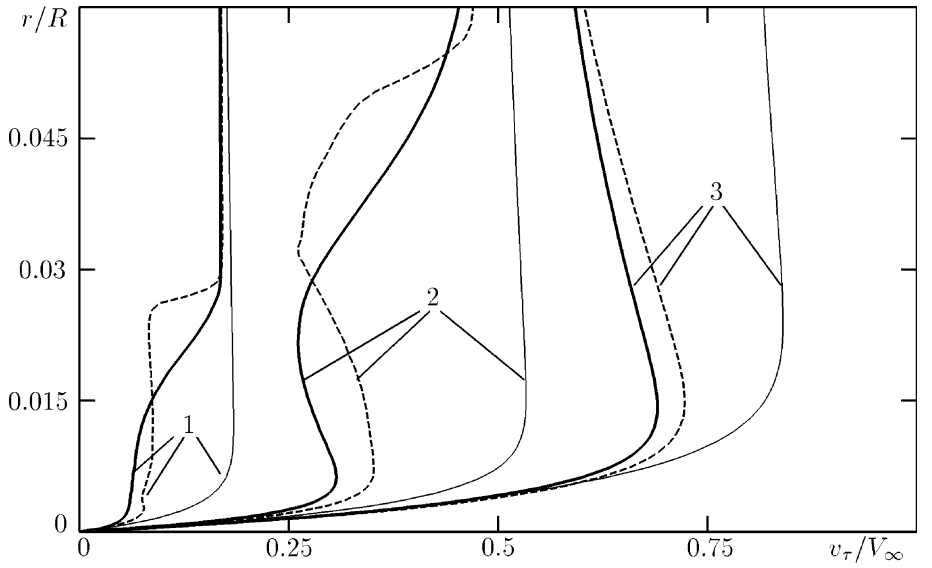

Fig. 8. Distribution of tangential velocity v_τ in different boundary layer cross-sections. Thin curves, pure gas flow ($\alpha_{p\infty} = 0$); thick curves, $r_p = 0.5$ μm, $\alpha_{p\infty} = 10^{-5}$, with collisions between particles; dashed curves, $r_p = 0.5$ μm, $\alpha_{p\infty} = 10^{-5}$, without collisions between particles. Curves 1, $\theta = 15°$; 2, $\theta = 45°$; 3, $\theta = 75°$ (angle θ is shown in Fig. 5(a)).

$\theta \leqslant \pi/4$. In the thin layer adjacent to the surface, the gas velocity v_τ decreases due to the collisions. At higher wall distance this velocity is increased by the collisions, up to the region far from the surface where reflected and chaotically moving particles are absent and collisions do not occur, as can be seen from the thick and dashed curves 1 which coincide far from the surface.

The modification of the carrier gas flow field causes an increase in the gas pressure p and viscous friction stress $\tau_w = \mu \partial v_\tau / \partial r$ at the body surface. This is illustrated by Fig. 9 in which the

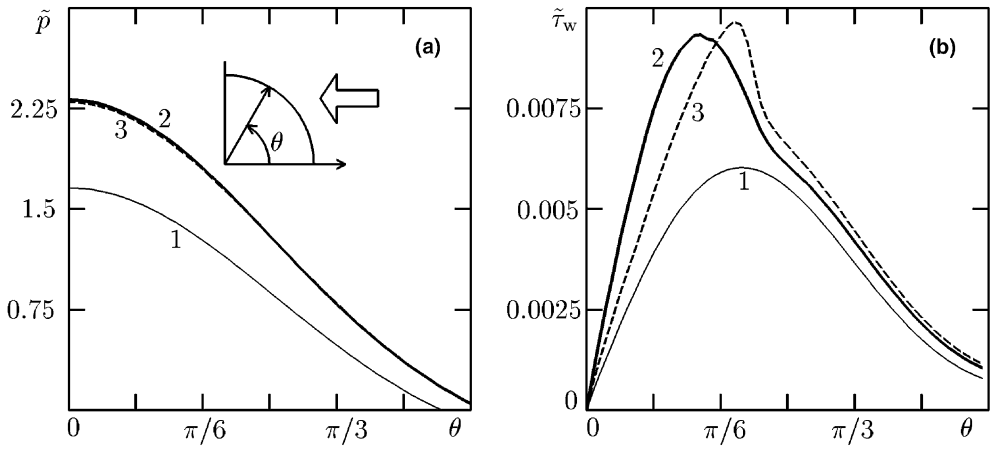

Fig. 9. Distribution of (a) pressure coefficient $\tilde{p} = 2(p - p_\infty)/(\rho_\infty V_\infty^2)$ and (b) friction coefficient $\tilde{\tau}_w = 2\tau_w/(\rho_\infty V_\infty^2)$ along the cylinder surface. Thin curve 1, pure gas flow ($\alpha_{p\infty} = 0$); thick curve 2, $r_p = 0.5$ μm, $\alpha_{p\infty} = 10^{-5}$, with collisions between particles; dashed curve 3, $r_p = 0.5$ μm, $\alpha_{p\infty} = 10^{-5}$, without collisions between particles.

distributions of the pressure coefficient $\tilde{p} = 2(p - p_\infty)/(\rho_\infty V_\infty^2)$ and the friction coefficient $\tilde{\tau}_w = 2\tau_w/(\rho_\infty V_\infty^2)$ along the cylinder contour are presented for the pure gas flow (curves 1) and for the flow of gas–particle mixture (curves 2 and 3). It is also seen that taking the inter-particle collisions into account in the flow model practically does not change the pressure and has a pronounced effect on the friction distribution. Due to collisions, $\tilde{\tau}_w$ increases near the stagnation region up to $\theta \approx 30°$ and decreases downstream.

4.4. Estimation of turbulence generation by particles

In steady-state 2D-flow Eq. (36) can be simplified to the form

$$\frac{\partial}{\partial x}(\langle\rho\rangle u_x k) + \frac{\partial}{\partial y}(\langle\rho\rangle u_y k) = \frac{\partial}{\partial x}\left(\langle\rho\rangle v_k \frac{\partial k}{\partial x}\right) + \frac{\partial}{\partial y}\left(\langle\rho\rangle v_k \frac{\partial k}{\partial y}\right) - \frac{2}{3}\langle\rho\rangle k\left(\frac{\partial u_x}{\partial x} + \frac{\partial u_y}{\partial y}\right) + 2\langle\rho\rangle v_t\left(\left(\frac{\partial u_x}{\partial x}\right)^2 + \left(\frac{\partial u_y}{\partial y}\right)^2 + \frac{1}{2}\left(\frac{\partial u_x}{\partial y} + \frac{\partial u_y}{\partial x}\right)^2\right) + \Pi_k - \langle\rho\rangle \frac{k^{3/2}}{l_{mp}}\left(1 + 2\frac{k}{\gamma\Re\langle T\rangle}\right), \tag{38}$$

where $u_x = \langle v_x\rangle$, $u_y = \langle v_y\rangle$. To estimate the distribution of k along the stagnation streamline $y = 0$ using the preliminary computed fields of the average variables, we assume that the diffusion of k in the y-direction in the plane of symmetry is negligible, i.e. $\partial(\langle\rho\rangle v_k \partial k/\partial y)/\partial y = 0$, and expand the variables in Eq. (38) in terms of the y-coordinate taking into account the symmetry conditions: $k = k_0(x) + k_2(x)y^2 + \ldots$, and similarly for u_x, $\langle\rho\rangle$,$\langle T\rangle$,Π_k and α_p; for u_y, we write $u_y = u_{y1}(x)y + u_{y3}(x)y^3 + \ldots$ Substituting these series for the variables into Eq. (38) and taking $y = 0$ we obtain an ordinary differential equation for $k_0(x)$, which is solved assuming that k_0 is equal to zero at the body surface and just after the shock wave: $k_0(x) = 0$ at $x = -R$ and $x = -(\Delta_s + R)$, where Δ_s is the distance between the bow shock and the cylinder along the stagnation streamline.

Results for the average fluctuating velocity of the fluid, $v'_{rms} = \sqrt{2k/3}$, are displayed in Fig. 10(a) and (b), for various r_p at fixed $\alpha_{p\infty}$ and for various $\alpha_{p\infty}$ at fixed r_p, respectively. Generation of turbulent kinetic energy can be seen to take place just behind the shock wave. For small particles, the level of velocity fluctuations is maximum at this location, and then decreases towards the cylinder wall, due to the high dissipation rate associated with such small size particles. On the contrary, the turbulence generated by larger particles is observed to slightly increase from the shock wave towards the stagnation point, except in the boundary layer, as a result of particle inertia leading to smaller deceleration and thus to higher relative velocity. It must be emphasized that the mean relative velocity between fluid and particles just after the shock wave does not depend on the particle diameter since all particles have the same velocity outside the shock layer and therefore also just behind the shock. This is the explanation of the peak observed in Fig. 10 for small particles, keeping in mind that for constant relative velocity, the turbulent kinetic energy source term in inversely proportional to the particle relaxation time, according to Eq. (28). In any case, from the proposed estimation the maximum turbulence intensity is found to be about 2% for $\alpha_{p\infty} = 10^{-5}$ (Fig. 10) and about 3% for $\alpha_{p\infty} = 3 \times 10^{-5}$. The effect of such

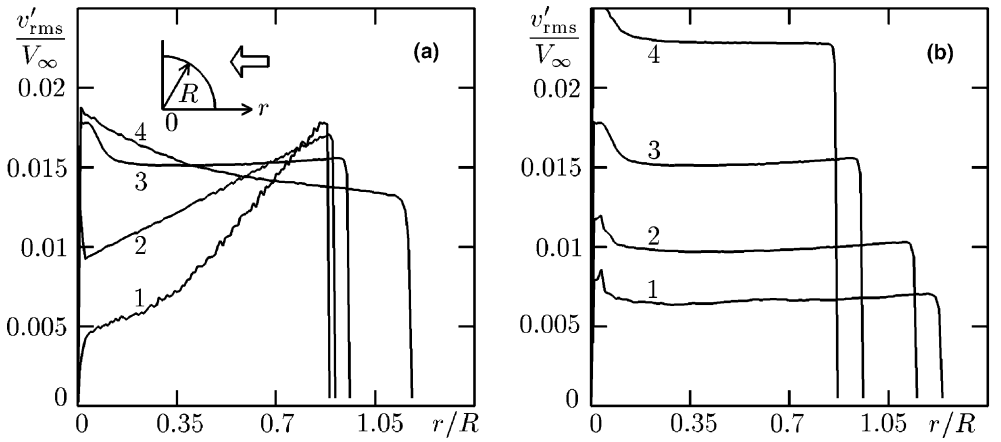

Fig. 10. Distribution of estimated rms velocity fluctuation of the gas $v'_{\rm rms} = \sqrt{(2/3)k}$ along the stagnation streamline. (a), $\alpha_{p\infty} = 10^{-5}$, curve 1, $r_p = 0.3$ μm; 2, $r_p = 0.5$ μm; 3, $r_p = 1$ μm; 4, $r_p = 3$ μm. (b), $r_p = 1$ μm, curve 1, $\alpha_{p\infty} = 10^{-6}$; 2, $\alpha_{p\infty} = 3\times10^{-6}$; 3, $\alpha_{p\infty} = 10^{-5}$; 4, $\alpha_{p\infty} = 3\times10^{-5}$.

fluctuations of the gas velocity upon the particle motion may be quantified by assessing the corresponding rms velocity of the solid particles, $v'_{\rm rms,t}$. A crude estimation can be obtained by means of the Tchen-Hinze formula expressing the particle velocity variance in terms of the fluid one (see e.g., Simonin, 1990). For $\rho_p^\circ \gg \rho$, this formula can be written:

$$(v'_{\rm rms,t})^2 = (v'_{\rm rms})^2 \frac{1}{1+\tau_p/\tau}, \tag{39}$$

where τ_p is the particle relaxation time, defined by $|\mathbf{f}_D| = m_p|\mathbf{v}-\mathbf{v}_1|/\tau_p$, and τ is the integral time scale of the fluid along the particle path, which is assimilated here to the fluid Lagrangian time scale and approximated by $\tau \approx 0.2k/\varepsilon$. Since this estimation of τ does not account for the crossing trajectory effect due to the mean relative velocity, the obtained value of $v'_{\rm rms,t}$ can be expected to overestimate the particle rms velocity induced by the gas turbulence. Applying Eq. (39) with the numerically predicted rms velocity of the gas, the particle turbulent intensity is found to be approximately constant within the shock layer, as shown by Fig. 11(a). The maximum value of $v'_{\rm rms,t}/V_\infty$ which is obtained for the smallest particles, is about 3.5×10^{-3}. From such an estimation, we can conclude that the effect of turbulence generated by particles is low enough for the assumptions made in Section 2.4 to be valid.

In the calculations described in Sections 4.2 and 4.3, the particles move chaotically due to random collisions between them. The root mean square velocity fluctuations of particles due to collisions $v'_{\rm rms,c}$ can be calculated formally as one of the macroparameters of the dispersed phase using the average operator (8)

$$(v'_{\rm rms,c})^2 = [(\mathbf{v}_1 - \mathbf{u}_p)^2]_1 = [\mathbf{v}_1^2] - \mathbf{u}_p^2. \tag{40}$$

However, particle trajectories could intersect with each other even if the particles move without collisions.

Therefore $v'_{\rm rms,c}$ calculated from (40) is not equal to zero even in collisionless particle phase flow. In order to get a quantity which could characterize the actual chaotic motion of particles due to

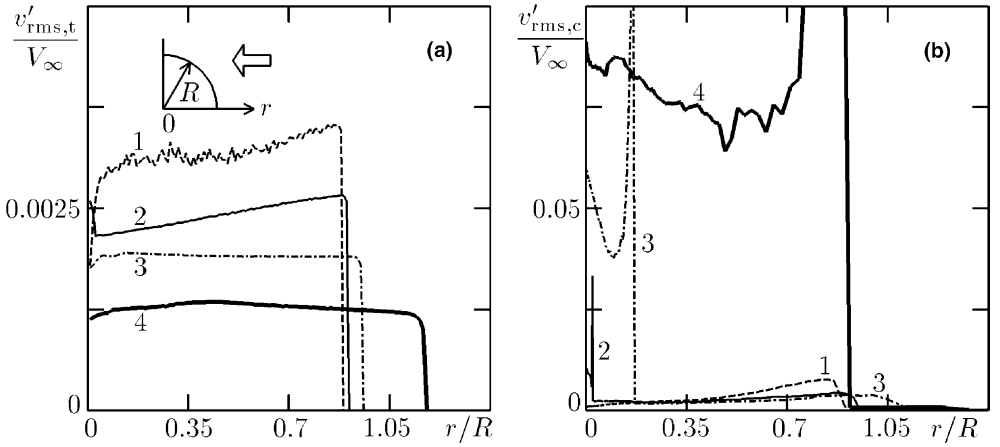

Fig. 11. Distribution along the stagnation streamline of estimated rms velocity fluctuation of particles due to (a) gas turbulence and (b) inter-particle collisions. $\alpha_{p\infty} = 10^{-5}$, curve 1, $r_p = 0.3$ μm; 2, $r_p = 0.5$ μm; 3, $r_p = 1$ μm; 4, $r_p = 3$ μm.

collisions, we define $v'_{\mathrm{rms,c}}$ as the rms velocity fluctuation of particles which undergo one or more collisions with other particles; in this case the velocity $\mathbf{u}_p$ in the right-hand side of (40) is the macroscopic velocity of these particles. The distributions of $v'_{\mathrm{rms,c}}$ along the stagnation streamline, shown in Fig. 11(b), are qualitatively similar to the distributions of particle concentration $\alpha_p/\alpha_{p\infty}$ in the case of collisionless motion of particles (see curve 5 in Fig. 2(a)). The maximum of $v'_{\mathrm{rms,c}}$ is observed near the envelope of the trajectories of particles reflected from the cylinder. Along the cylinder surface (not shown) the maximum of $v'_{\mathrm{rms,c}}/V_\infty$ is observed at $\theta > 45°$ and it is about 17% for particles of radius $r_p = 3$ μm and about 8% for $r_p = 1$ μm. Comparison of the levels of $v'_{\mathrm{rms,t}}$ and $v'_{\mathrm{rms,c}}$ displayed in Fig. 11 shows that the rms velocity fluctuation of particles due to collisions $v'_{\mathrm{rms,c}}$ is one order of magnitude higher than the estimated rms velocity fluctuation of particles due to turbulence $v'_{\mathrm{rms,t}}$, except for very fine particles of subcritical radius $r_p = 0.3$ μm.

5. Conclusion

A model of viscous two-phase gas–particle flow over a blunt body has been presented. It takes into account the inter-particle collisions and the reverse action of the dispersed phase on the carrier gas flow. The models used for gas–particle interaction, particle–particle collisions and particle–wall collisions are described in detail. It should be noted that at present some parameters entering the flow model, for example the restitution coefficients a_{rn} and a_{rt} in the particle–particle collision model, can only be estimated but cannot be determined with the desirable accuracy neither from physical experiments nor from mathematical or numerical modeling. Nevertheless, some definite conclusions on many key features of the flow considered could be drawn from the results of the computational simulation.

The numerical study of the dispersed phase and carrier gas flow fields has allowed us to find the ranges of particle radius r_p and free stream particle volume fraction $\alpha_{p\infty}$ in which the inter-particle collisions and the two-way coupling effects play a significant role, and also to understand how the inter-particle collisions modify the flow structure and some important parameters of both phases.

The typical flow patterns of both phases in the shock layer and, in particular, inside the boundary layer have been described. Besides, the gas turbulent kinetic energy generated by particles as well as the kinetic energy of chaotic motion of particles caused by the flow turbulence have been estimated. The last has been found to be much less than the kinetic energy of the particle chaotic motion caused by inter-particle collisions.

The collisions between large particles, i.e. in the range of $r_p \geqslant 1$ μm in the flow considered, have a noticeable effect on the flow of the two-phase mixture at very low particle volume fraction. When $\alpha_{p\infty}$ increases from extremely low values, the collisions first modify the dispersed phase flow structure (at $\alpha_p \gtrsim 10^{-6}$), and only at much higher particle volume fraction ($\alpha_p \gtrsim 10^{-5}$) they have a pronounced effect on the carrier gas flow field. This result is in complete agreement with the apriori estimates obtained earlier (see Section 1). However, for particles whose radius is close but slightly larger than the critical value r_{p*}, both effects become essential simultaneously with increasing $\alpha_{p\infty}$. Gas–solid flows over bodies with particles of near-critical radius were not studied earlier at all. The concentration of such particles near the stagnation point is several times higher than for coarse-grained particles at the same value of $\alpha_{p\infty}$, and such particles have a more strong effect on the gas flow, particularly on the heat flux from the gas to the body surface. The question of how particles modify the gas phase heat flux is very important in many applications, but it is still open and has to be the subject of further study.

Acknowledgement

The authors are grateful to the INTAS for the financial support of this study through the grant No. 00-0309.

References

Babukha, G.L., Shraiber, A.A., 1972. Interaction of Polydisperse Particles in Two-Phase Flows. Naukova Dumka, Kiev (in Russian).

Berlemont, A., Desjonqueres, P., Gouesbet, G., 1990. Particle Lagrangian simulation in turbulent flows. Int. J. Multiphase Flow 16, 19–34.

Bird, G.A., 1994. Molecular Gas Dynamics and the Direct Simulation of Gas Flows. Clarendon Press, Oxford, New York.

Boulet, P., Moissette, S., 2002. Influence of particle-turbulence modulation modelling in the simulation of non-isothermal gas–solid flow. Int. J. Heat Mass Transfer 45, 4201–4216.

Crowe, C.T., 1982. Review—numerical models for dilute gas–particle flows. Trans. ASME, J. Fluids Engng. 104, 297–303.

Crowe, C.T., 2000. On models for turbulence modulation in fluid–particle flows. Int. J. Multiphase Flow 26, 719–727.

Crowe, C.T., Sommerfeld, M., Tsuji, Y., 1998. Multiphase Flows with Droplets and Particles. CRC Press, Boca Raton.

Dennis, S.C.R., Singh, S.N., Ingham, D.B., 1980. The steady flow due to a rotating sphere at low and moderate Reynolds numbers. J. Fluid Mech. 101, 257–279.

Elghobashi, S.E., Abou-Arab, T.W., 1983. A two-equation turbulence model for two-phase flows. Phys. Fluids A 26, 931–938.

Fuchs, N.A., 1964. The Mechanics of Aerosols. Pergamon Press, New York.

Golovachov, Yu.P., Schmidt, A.A., 1980. Supersonic dusty gas flows about blunted bodies. Ioffe Physical Technical Institute of the USSR Academy of Sciences, Paper No. 690. LIYaF, Leningrad (in Russian).

Henderson, C.B., 1976. Drag coefficients of spheres in continuum an rarefied flows. AIAA J. 14, 707–708.
Ishii, R., Hatta, N., Umeda, Y., Yuhi, M., 1990. Supersonic gas–particle two-phase flow around a sphere. J. Fluid Mech. 221, 453–483.
Ivanov, M.S., Rogazinsky, S.V., 1988. Comparative analysis of DSMC techniques in rarefied gas dynamics. Z. Vychislitelnoi Mate. Mate. Fiz. 28, 1058–1070 (in Russian).
Kenning, V.M., Crowe, C.T., 1997. Effect of particles on carrier phase turbulence in gas–particle flow. Int. J. Multiphase Flow 23, 403–408.
Kitron, A., Elperin, T., Tamir, A., 1988. Monte Carlo analysis of wall erosion and direct contact heat transfer by impinging two-phase lets. J. Thermophys. 3, 112–122.
Kogan, M.N., 1967. Rarefied Gas Dynamics. Nauka, Moscow (in Russian).
Lashkov, V.A., 1991. Experimental determination of the coefficients of restitution of particles in the flow of a gas suspension in a collision against the surface. J. Engng. Phys. 60, 154–159.
Nigmatulin, R.I., 1990. Dynamics of Multiphase Media, vol. 1. Hemisphere, New York.
Oesterlé, B., Bui Dinh, T., 1998. Experiments on the lift of a spinning sphere in a range of intermediate Reynolds numbers. Exp. Fluids 25, 16–22.
Oesterlé, B., Petitjean, A., 1993. Simulation of particle-to-particle interactions in gas–solid flows. Int. J. Multiphase Flow 19, 199–211.
Osiptsov, A.N., 1985. Boundary layer on a blunt body in a dusty gas flow. Izv. Akad. Nauk SSSR, Mekh. Zhidk. Gaza., 99–107.
Ramm, M.S., 1988. Numerical investigation of the structure of the two-phase shock layer near the forward part of a blunt body in a supersonic flow. Ph.D. thesis, Leningrad Polytechnical Institute, Leningrad, USSR (in Russian).
Rubinow, S.I., Keller, J.B., 1961. The transverse force on a spinning sphere moving in viscous fluid. J. Fluid Mech. 11, 447–459.
Sakiz, M., Simonin, O., 2001. Continuum modelling and Lagrangian simulation of massive frictional colliding particles in a vertical gas–solid channel flow. In: Michaelides, E. (Ed.), Proc. 4th Int. Conf. on Multiphase Flow. New Orleans, USA, (CD-ROM Proc. ICMF'2001, Paper 186).
Sarkar, S., Balakrishnan, L., 1990. Application of a Reynolds-stress turbulence model to the compressible shear layer. ICASE Report 90-18, NASA CR 182002.
Simonin, O., 1990. Eulerian formulation for particle dispersion in turbulent two-phase flows. In: Sommerfeld, M., Wennerberg, D. (Eds.), Proc. 5th Workshop on Two-Phase Flow Predictions, Erlangen, Germany, pp. 156–166.
Simonin, O., Squires, K.D., 2001. On turbulence modification in dense particulate two-phase flows. EUROMECH Colloquium 421 on Strongly-Coupled Dispersed Two-Phase Flows, Grenoble, France.
Sommerfeld, M., 1995. The importance of inter-particle collisions in horizontal gas–solid channel flow. In: Stock, D.E. et al. (Eds.), Gas–Particle Flows. ASME FED-Vol. 228, 335–345.
Sommerfeld, M., 2001. Validation of a stochastic Lagrangian modelling approach for inter-particle collisions in homogeneous isotropic turbulence. Int. J. Multiphase Flow 27, 1829–1858.
Sternin, L.E., Shraiber, A.A., 1994. Multiphase flows of gas with particles. Mashimostroeniye, Moscow (in Russian).
Sun, J., Chen, M.M., 1988. A theoretical analysis of heat transfer due to particle impact. Int. J. Heat Mass Transfer 31, 969–974.
Tanaka, T., Tsuji, Y., 1991. Numerical simulation of gas–solid two-phase flow in a vertical pipe: on the effect of inter-particle collision. In: Stock, D.E. et al. (Eds.), Gas–Solid Flows. ASME FED, vol. 121, pp. 123–128.
Tsirkunov, Yu.M., 1993. Admixture flow modeling in problems of two-phase aerodynamics. Boundary layer effects. Modeling in Mechanics 7, 151–193 (in Russian).
Tsirkunov, Yu.M., Tarasova, N.V., Volkov, A.N., 1994a. Boundary layer effects in the dusty gas flow over a blunt body. In: EUROMECH Colloquium 319, May 17–20, 1994, Tallinn, Estonia, Proc. Estonian Acad. Sci. Phys. Math. 43 (4), 250–262.
Tsirkunov, Yu.M., Panfilov, S.V., Klychnikov, M.B., 1994b. Semiempirical model of impact interaction of a disperse impurity particle with a surface in a gas suspension flow. J. Engng. Phys. Thermophys. 67, 1018–1025.
Tsirkunov, Yu.M. 2001. Gas–particle flows around bodies—key problems, modeling and numerical analysis. In: Michaelides, E. (Ed.), Proc. 4th Int. Conf. Multiphase Flow. New Orleans, USA (CD-Rom Proc. ICMF'2001, paper 609).

Tsirkunov, Yu.M., Volkov, A.N., Tarasova, N.V., 2002. Full Lagrangian approach to the calculation of dilute dispersed phase flows: advantages and applications. In: CD-ROM Proc. ASME FEDSM'02, Montreal, Canada, paper 31224.

Vasilevskii, E.B., Osiptsov, A.N., Chirikhin, A.V., Yakovleva, L.V., 2001. Heat transfer at the forward surface of a blunt body in a high speed flow containing low-inertial particles. Inz.-Fiz. Z. 74, 29–37 (in Russian).

Volkov, A.N., Tsirkunov, Yu.M., 1996. Direct simulation Monte-Carlo modelling of two-phase gas–solid particle flows with inelastic particle–particle collisions. In: Proc. Third ECCOMAS Comp. Fluid Dynamics Conf., Paris, France, pp. 662–668.

Volkov, A.N., Tsirkunov, Yu.M., 2000. Kinetic model of a collisional admixture in dusty gas and its application to calculating flow past bodies. Izv. Russ. Akad. Nauk, Mekh. Zhidk. Gasa, 81–97 (Engl. transl. Fluid Dynamics 35 (3), 380–392).

Volkov, A.N., Tsirkunov, Yu.M., 2002. CFD/Monte Carlo simulation of collision-dominated gas–particle flows over bodies. In: CD-ROM Proc. ASME FEDSM'02, Montreal, Canada, paper 31222.

Yee, H.C., Harten, A., 1987. Implicit TVD schemes for hyperbolic conservation laws in curvilinear coordinates. AIAA J. 25, 266–274.

Zhou, Y., Wexler, A.S., Wang, L.-P., 1998. On the collision rate of small particles in isotropic turbulence. II. Finite inertia case. Phys. Fluids 10, 1206–1216.